SERI/TR-252-1951
DE85000509

September 1984

OR#0626-2

I-18228

Performance of the SERI Parallel-Passage Dehumidifier

Dennis Schlepp
Robert Barlow

DO NOT MICROFILM
COVER

SERI

Solar Energy Research Institute
A Division of Midwest Research Institute

1617 Cole Boulevard
Golden, Colorado 80401

Operated for the
U.S. Department of Energy
under Contract No. DE-AC02-83CH10093

DISCLAIMER

This report was prepared as an account of work sponsored by an agency of the United States Government. Neither the United States Government nor any agency thereof, nor any of their employees, makes any warranty, express or implied, or assumes any legal liability or responsibility for the accuracy, completeness, or usefulness of any information, apparatus, product, or process disclosed, or represents that its use would not infringe privately owned rights. Reference herein to any specific commercial product, process, or service by trade name, trademark, manufacturer, or otherwise does not necessarily constitute or imply its endorsement, recommendation, or favoring by the United States Government or any agency thereof. The views and opinions of authors expressed herein do not necessarily state or reflect those of the United States Government or any agency thereof.

DISCLAIMER

Portions of this document may be illegible in electronic image products. Images are produced from the best available original document.

SERI/TR-252-1951
UC Category: 59a
DE85000509

SERI/TR--252-1951

DE85 000509

Performance of the SERI Parallel-Passage Dehumidifer

Dennis Schlepp
Robert Barlow

September 1984

DISCLAIMER

This report was prepared as an account of work sponsored by an agency of the United States Government. Neither the United States Government nor any agency thereof, nor any of their employees, makes any warranty, express or implied, or assumes any legal liability or responsibility for the accuracy, completeness, or usefulness of any information, apparatus, product, or process disclosed, or represents that its use would not infringe privately owned rights. Reference herein to any specific commercial product, process, or service by trade name, trademark, manufacturer, or otherwise does not necessarily constitute or imply its endorsement, recommendation, or favoring by the United States Government or any agency thereof. The views and opinions of authors expressed herein do not necessarily state or reflect those of the United States Government or any agency thereof.

Prepared under Task No. 1131.00
WPA No. 256

Solar Energy Research Institute
A Division of Midwest Research Institute

1617 Cole Boulevard
Golden, Colorado 80401

Prepared for the
U.S. Department of Energy
Contract No. DE-AC02-83CH10093

MASTER

DISTRIBUTION OF THIS DOCUMENT IS UNLIMITED

Blank Page

PREFACE

The DOE Active Solar Heating and Cooling Program's objective is to develop the technology base to allow the private sector to produce efficient, economically competitive solar technology options for the marketplace. The program is composed of a balance of research on systems, components, and materials. The systems research directs the program through analysis of alternative, advanced concepts in heating or cooling or both. Additionally, systems reliability research provides data on critical components and materials that affect long-term performance. The analysis and reliability programs are augmented by a laboratory and field test program that develops data on experimental and state-of-the-art systems. These data identify design and operational problems, and thus opportunities for research.

The Component and Materials Program performs research on advanced concepts that have been identified by systems analysis to offer promise of being competitive with conventional, nonrenewable energy sources. Key components, such as chillers, dehumidifiers, heat exchangers, and collectors, are evaluated for improved efficiency and cost through innovation in design. Advanced materials for these key components are evaluated and modified to provide improved performance and lower cost.

This report documents the design, construction, and testing of dehumidifier prototypes for solar desiccant cooling systems, using a parallel-passage design for high performance and low pressure drop. The DESSIM computer model for predicting performance of desiccant dehmidifiers was modified to account for the new geometry and was validated through comparison with the experimental data for single-blow adsorption and desorption. Predictions are made of steady-state system performance using the new design.

This research was performed under task 1131.00, Desiccant Cooling Research, during FY 1982. The authors would like to express their appreciation to Harry Pohl, laboratory technician, and Guido Terziotti, summer intern, for their work during the experimental phase of the work, and to Terry Penney for his assistance and review of the design and experimental work.

Dennis Schlepp
Dennis Schlepp
Thermal Sciences Research Branch

Approved for:

SOLAR ENERGY RESEARCH INSTITUTE

David H. Johnson
David Johnson, Acting Manager
Thermal Sciences Research Branch

L. J. Shannon, Director
Solar Heat Research Division

SUMMARY

Objective

To characterize the performance of a parallel-passage dehumidifier geometry in single-blow operation and to update current models of dehumidifier performance using this experimental data.

Discussion

The key component in improving the performance of solar desiccant cooling systems is the dehumidifier. A parallel-passage geometry for the desiccant dehumidifier has been identified as meeting key criteria of low pressure drop, high mass transfer efficiency, and compact size. An experimental program to build and test a small-scale prototype of this design was undertaken in FY 1982, and the results are presented in this report. Computer models to predict the adsorption/desorption behavior of desiccant dehumidifiers were updated to take into account the geometry of the bed and predict potential system performance using the new component design.

Conclusions and Recommendations

A parallel-passage design proved to have high mass transfer effectiveness and low pressure drop over a wide range of conditions typical of desiccant cooling system operation. The prototype dehumidifier averaged 93% effectiveness at pressure drops of less than 50 Pa at design point conditions.

Predictions of system performance using models validated with the experimental data indicate that system thermal coefficients of performance (COPs) of 1.0 to 1.2 and electrical COPs above 8.5 are possible using this design.

The success of this basic dehumidifier geometry in meeting the needs of performance in solar desiccant cooling systems points the way to further research. First, cyclic testing of the basic design will provide valuable information on the heat and mass transfer characteristics of desiccant dehumidifiers in system operation. Second, work in basic heat and mass transfer mechanisms, such as sorption hysteresis and resistances to water transport, is needed to fully understand the processes taking place in the dehumidifier component.

TABLE OF CONTENTS

LIST OF FIGURES

LIST OF TABLES

SECTION 1.0

INTRODUCTION

1.1 BACKGROUND

Research in desiccant cooling under the U.S. Department of Energy (DOE) Office of Solar Heat Technologies' Active Heating and Cooling Program has proceeded for about six years. Three desiccant cooling prototypes (AiResearch, IGT, and IIT), representing the first generation of systems, have been built and tested with thermal coefficients of performance (COPs) ranging from 0.5 to 0.6 kW cooling output/kW thermal input [1,2,3]. An economic evaluation of solar technologies [4] indicated that these COPs must be at least doubled before desiccant cooling systems could be competitive with conventional vapor compression cooling systems. Detailed simulations using a desiccant computer model (DESSIM) developed at SERI [5] have demonstrated that COPs above 1.0 can be achieved using high-effectiveness components in a ventilation mode. In particular, the effectiveness of the sensible heat exchanger should be increased from the 0.89-0.90 range found in the prototypes to about 0.95. Similar performance levels should be sought in the dehumidifier.

State-of-the-art dehumidifiers are less advanced than state-of-the-art heat exchangers, so the greatest potential for increasing desiccant system performance appears to lie in the development of high-performance, low-pressure-drop dehumidifiers. The report entitled An Assessment of Dehumidifier Geometries for Desiccant Cooling Systems [6] discusses the basic principles of heat and mass transfer in dehumidifiers and gives a technical evaluation of five dehumidifier designs. The wound-ribbon dehumidifier is identified as the most promising design, and preliminary computer predictions of a system using this design give a design point COP near 1.1. Accordingly, the wound-ribbon dehumidifier design was chosen for construction and testing.

1.2 TECHNICAL APPROACH AND SCOPE

The predicted system COP given above was obtained using a version of the DESSIM program. This code was originally developed for the study of packed-bed, silica gel dehumidifiers, and it was validated for packed beds through comparison with experimental data on single-blow absorption and desorption from the Desiccant Test Laboratory at SERI [5,7]. (Single blow refers to a step change in inlet air conditions that is imposed on a desiccant bed having uniform initial conditions of temperature and moisture content.) The primary objective of the experimental work documented in this report was to provide data on the heat and mass transfer characteristics of the new wound-ribbon dehumidifier so that the corresponding version of DESSIM could be validated or modified appropriately to give accurate predictions of dehumidifier performance. This is done by comparing measured and predicted outlet air temperature and humidity as functions of time during single-blow absorption or desorption. It is assumed that if the computer model accurately predicts single-blow results it can be used to predict the performance of the same dehumidifier operating within a cooling system.

Our approach was to design and build a wound-ribbon dehumidifier with dimensions and materials that would be representative of those that might be used in a full-scale cooling system. Simulations using DESSIM were used to determine qualitative effects of variation of some parameters; e.g., the mass fraction of silica gel in the ribbon. However, we did not attempt to optimize the design at this stage, and many design decisions were based on the availability of materials. Once the first dehumidifier had been successfully tested an aggressive schedule was adopted to build and test three additional dehumidifiers with different silica gel particle size and/or ribbon spacing, two important design parameters.

The air loop in the Desiccant Test Laboratory was used as described in Ref. [7] with only minor modifications. The test section was rebuilt to accommodate the new dehumidifier modules. Instrumentation was upgraded to reduce uncertainties in measured quantities, and data acquisition software was improved.

Details of the design and construction of the dehumidifier are given in Section 2.0. The desiccant test loop and modifications to it are described in Section 3.0. Section 4.0 discusses the DESSIM simulation program and outlines the equations used to analyze the wound-ribbon geometry. Experimental results are discussed in Section 5.0. Results of computer simulations of system performance are given in Section 6.0, and Section 7.0 contains conclusions and recommendations for future research.

SECTION 2.0

DEHUMIDIFIER DESIGN AND CONSTRUCTION

2.1 THE CONCEPT

The wound-ribbon dehumidifier is made with a thin polyester sheet coated on both sides with a single layer of small silica gel particles to produce a sandpaper-like surface. This sheet or ribbon is then tension-wound into a wheel. Spacers are inserted between successive layers of the ribbon during the winding process and are held in place by radial spokes on each face of the wheel. These spacers form narrow, parallel-walled, laminar-flow passages that allow air to flow through the matrix in the axial direction. The result is a compact, high-effectiveness, low-pressure-drop heat and mass exchanger for dehumidification.

This wound-ribbon dehumidifier is based on a combination of concepts developed by researchers at Commonwealth Scientific and Industrial Research Organization (CSIRO) in Australia and at the University of California at Los Angeles (UCLA). Wound polyester ribbon heat exchangers were developed at CSIRO in the 1960s, and they have since been manufactured by Rotary Heat Exchangers Pty. Ltd. in Melbourne for use as energy recovery wheels in building ventilation systems [8]. Researchers at UCLA [9,10] developed the concept of using a sandpaper-like coating of silica gel particles on the walls of laminar flow channels. They built and tested a fixed-bed dehumidifier element with relatively thick plastic sheets between the flow channels.

Combining these ideas results in a dehumidifier with several advantages over previous dehumidifier designs. First, the parallel-walled, laminar-flow geometry has the highest ratio of Stanton number to friction factor known to the authors. This nondimensional ratio is a measure of the ratio of heat and mass transfer performance to pressure drop that can be expected from the device for given dimensions and flow rates. Second, the mass transfer resistance associated with diffusion of moisture into and out of the solid matrix is minimized by exposing small desiccant particles directly to the air stream. Third, a high mass fraction of silica gel (above 0.5) can be achieved. This is important in maintaining cooling capacity as high as possible. Fourth, this dehumidifier is relatively simple to manufacture. Advantages and disadvantages of the wound-ribbon dehumidifier and four other dehumidifier designs are compared in detail in Ref. [6].

2.2 DEHUMIDIFIER DESIGN

The objective of this project was to test and analyze a wound-ribbon dehumidifier with dimensions and materials that would be representative of those that might be used in a full-scale cooling system. To allow sufficient time for testing, the first dehumidifier had to be designed and built within roughly a four-month period. Consequently, the design was kept as simple as possible, avoiding requirements for any items with long ordering lead times. We did not attempt to optimize the design at this stage with respect to parameters such as ribbon thickness, spacer thickness, or particle diameter.

Rather, ranges of reasonable values were identified with the assistance of computer simulations, and materials were selected on the basis of off-the-shelf availability or ease of in-house fabrication. The end result was very satisfactory, demonstrating the relative ease with which this type of dehumidifier could be produced on a large scale.

Details of the dehumidifier design, the materials used, and the machines built for coating the ribbon and winding the wheel are given in Sections 2.2.1 through 2.2.5. Materials are summarized in Table 2-1.

Specific heats of tape and plastics were measured with a differential scanning calorimeter in the Materials Branch at SERI. Uncertainties are roughly ±5% to ±10% based on repeatability of one of the scans. Specific heats for aluminum and silica gel are from Refs. [14] and [15], respectively.

2.2.1 Selection of Ribbon Materials

The ribbon comprises a plastic film substrate, an adhesive, and a layer of desiccant particles. Polyester film, 76-μm (0.003-in.) thick, is used in the construction of the Australian wound-ribbon heat exchangers. The high tensile strength of this plastic makes it well suited for tension winding, and we saw no reason to try any other material. Polyester or Mylar® film is readily available in several thicknesses from a variety of vendors. It comes in wide rolls but can be slit to desired widths prior to delivery.

Table 2-1. Summary of Dehumidifier Materials

Component	General Description	Dimensions	Specific Heat ($J/kg^{\circ}C$)
Tape	Mystik® 6466: 0.025-mm (0.001-in.) polyester film with thermosetting adhesive on both sides. Total thickness: 0.076 mm (0.003 in.)	0.20 m × 33 m (8 in. × 36 yd)	1690 at 30°C 1840 at 60°C
Desiccant	Silica gel ground from Davison® Grade 40 and sieved (60-80 mesh and 35-45 mesh)	180-250 μm and 355-500 μm	921
Hub	High-density polyethylene rod	5.1 cm in diameter	2370 at 30°C 2990 at 60°C 3880 at 90°C
Spokes	Aluminum channel	1.27 cm × 1.2 cm (0.5 in. × 0.5 in.) 0.24-cm (0.094-in.) wall	896
Spacers	High-density polyethylene	0.724 cm × 21.6 cm × 0.15 cm thick	1900 at 30°C 2400 at 60°C 3200 at 90°C

Silica gel was selected as the desiccant. Computational investigations of the effect of desiccant properties on system performance [11,12] have shown that even the most optimistic of hypothetical desiccant properties produce only a relatively small (roughly 10%) performance improvement, compared with silica gel. Several grades of silica gel are commercially available in grain sizes of interest. However, detailed absorption properties for individual grades are not available from the manufacturer. To avoid ambiguity in properties, we decided to grind and sieve our own silica gel from the supply of large-grain Davison Grade 40 gel that had been used in the packed-bed absorption tests. The properties of this gel have been relatively well characterized, and Rojas [13] measured the equilibrium properties of a sample from our stock of this gel. Small-scale equipment for grinding and sieving was available at SERI, and samples of silica gel of several grain sizes between 80 μm and 500 μm (200 mesh to 35 mesh) were produced.

Several options were considered for the actual production of the ribbon, including in-house production that involved coating polyester film with adhesive and applying a layer of silica gel. An alternative was to subcontract the ribbon production. We contacted the abrasives (sandpaper) division of 3M Co. (Minnesota Mining and Manufacturing). They could have done the job, but their production scale and time requirements would have posed significant project delays. Fortunately, we tried applying silica gel to a piece of pressure-sensitive packing tape and produced a very uniform and durable coating. After contacting several tape distributors, we identified a double-sided polyester tape manufactured by Mystik Tape Company that was appropriate, and samples were obtained.

Samples of this tape were coated with different grain sizes of silica gel. Figure 2-1 shows that there is an approximately linear relationship between

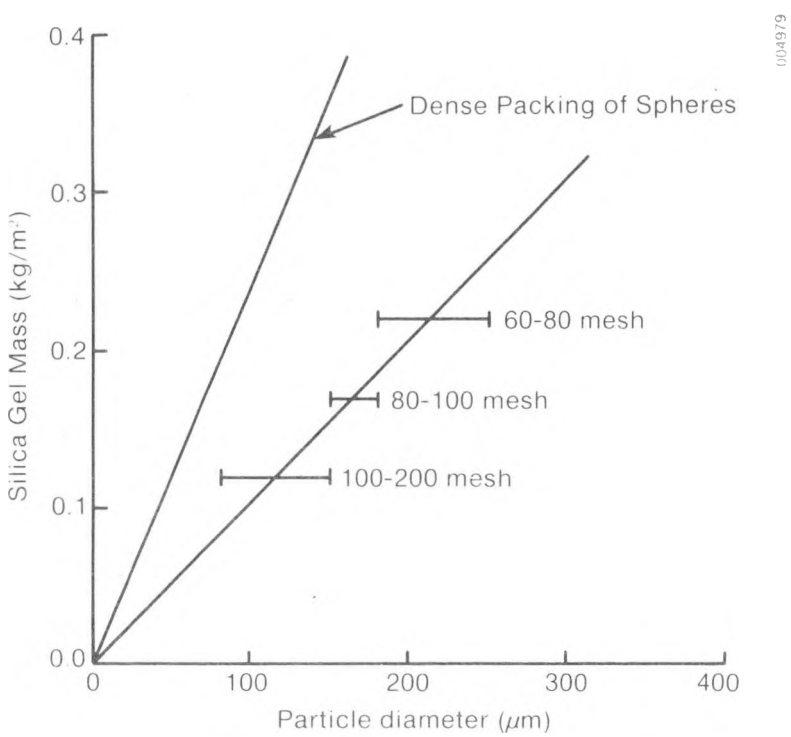

Figure 2-1. Silica Gel Grain Size versus Coated Tape Density

average grain size and the mass of silica gel (both sides coated) per unit of tape area. This is roughly 0.5 to 0.6 times the mass that would be obtained with a single layer of densely packed spheres as calculated in Ref. [9]. The fraction of silica gel mass to total ribbon mass is between 50% and 68% for the particle sizes being considered in this study. Figure 2-2 shows the predicted effect of this mass fraction on the capacity and COP of a cooling system. The first dehumidifier was designed for a silica gel fraction of about 60%, which represents a good compromise between COP and capacity.

Aging the ribbon samples over a four-day period at 95°C did not have any adverse effect on the adhesive bond, nor did it cause the tape to become brittle. This tape worked well for our purposes with no apparent deterioration over the testing period of several months. However, a tape with a thicker plastic substrate may be more appropriate for large-scale applications because of increased tolerance to stresses of winding.

2.2.2 Tape-Coating Device

Experience with small samples showed that it was relatively easy to obtain a uniform coating of silica gel on this tape simply by spreading the gel over the tape and brushing off the excess. A device was designed and built to facilitate the process for coating complete rolls of the tape (Fig. 2-3). The tape comes off its spool and is drawn through a bath of silica gel past several rollers and onto a manually driven take-up reel. Two brushes remove most of the excess gel, and funnels and tubes are used to feed silica gel to the bath. (There is no silica gel in the device shown in Fig. 2-3.)

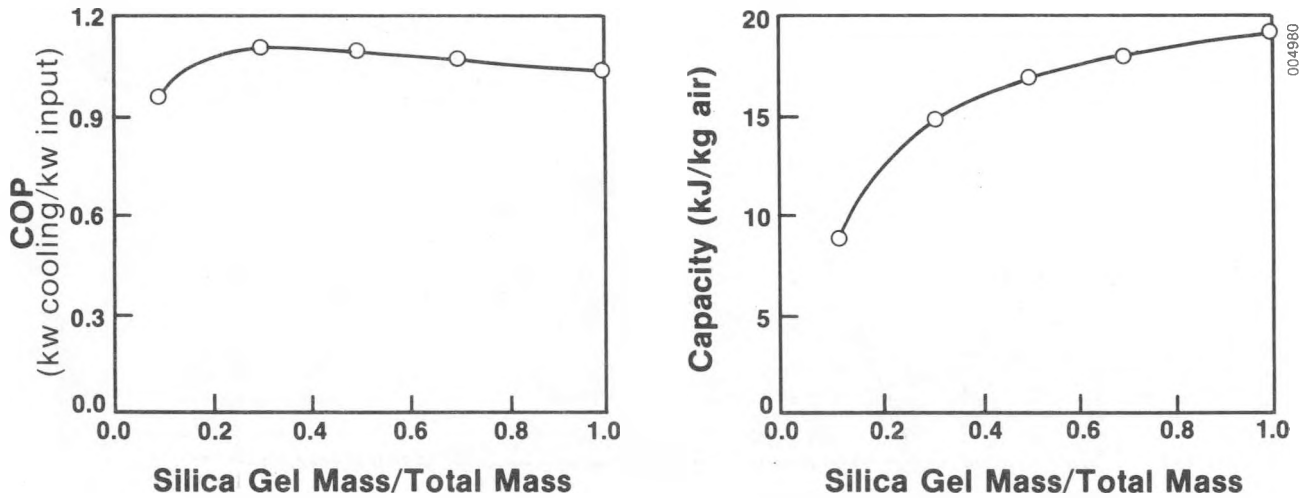

Figure 2-2. Coefficient of Performance and Specific Capacity versus Mass Fraction Silica Gel

2.2.3 Hub and Spoke Design

Design of these components was based to a large extent on the availability of materials. When rough design requirements were established, the materials summarized in Table 2-1 were selected. Figure 2-4 shows the hub and spoke assembly along with several spacers and an 8-in. roll of the double-sided tape. The 2-in.-diameter, high-density polyethylene hub has radial slots milled in each end for the spokes to fit into, and there is a slot along its length to allow anchoring of the tape. Eight radial spokes of 0.5-in. aluminum channel are bolted to each of two aluminum disks that form caps at each end of the hub. A bolt passes through the entire assembly to hold it

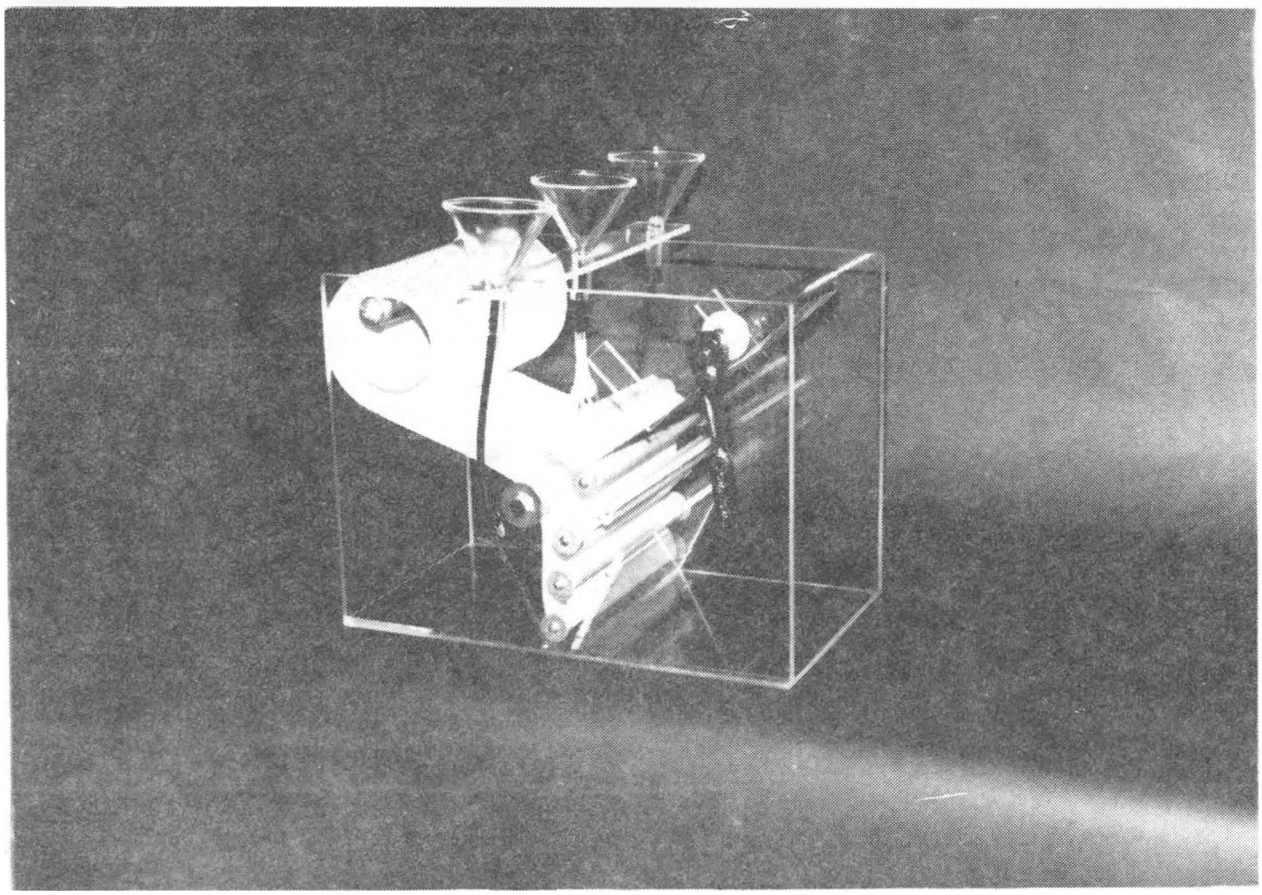

Figure 2-3. Tape-Coating Device

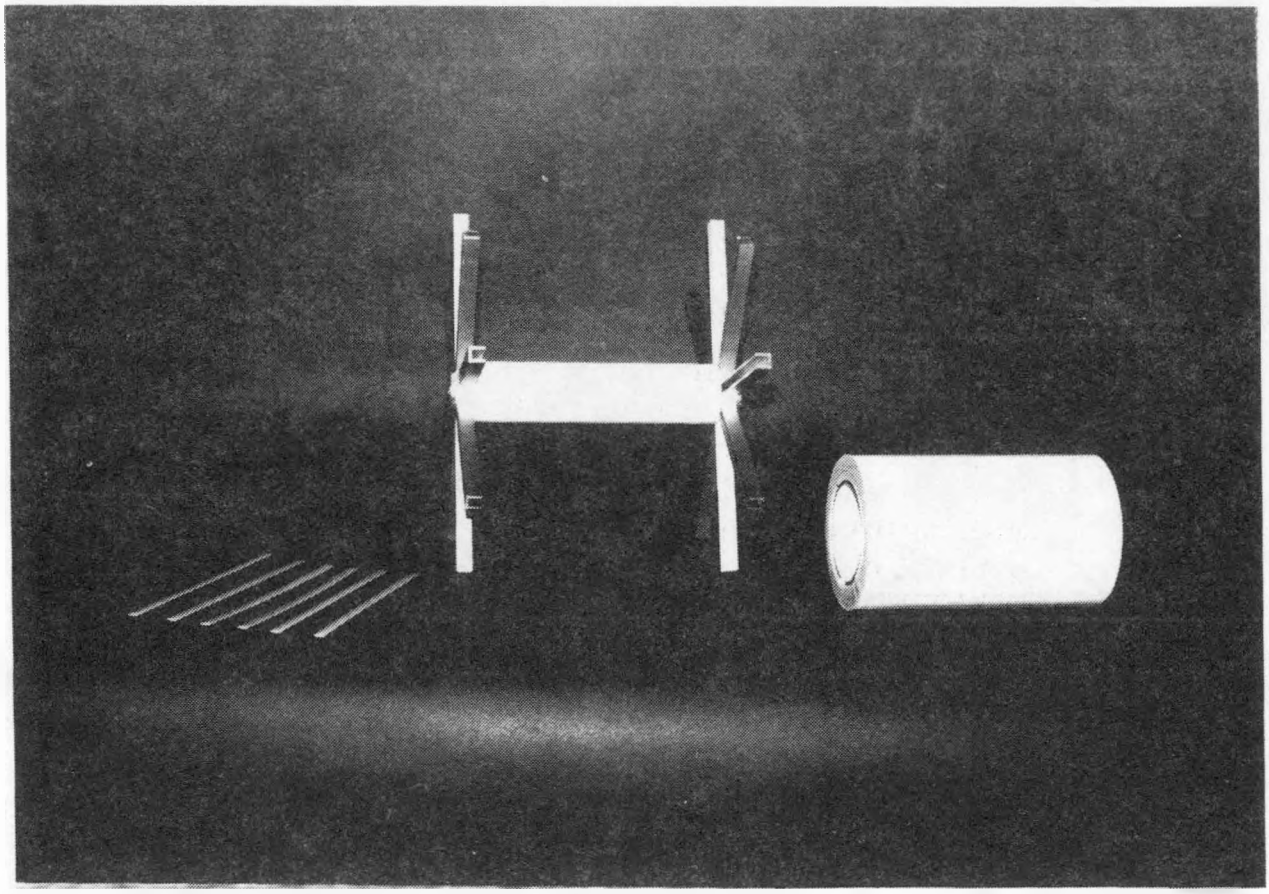

Figure 2-4. Hub and Spoke Assembly with Spacers and Tape Roll

together and to act as an axle during the winding process. The length of the hub allows about 1-mm clearance on each side of the ribbon, and the radius of the spokes is 29.8 cm (11.75 in.), which allows the assembly to slide into a standard 24-gauge sheet metal connector for the 12-in. spiral duct used in the test loop.

2.2.4 Spacers

A sheet metal cutter was used to cut spacers from large sheets of high-density polyethylene. Spacer thickness was determined by the availability of plastic sheets in the appropriate size range. The upper limit of this range was

determined by the Ntu (number of transfer units) requirements of the dehumidifier. If we assume a fixed void fraction in the dehumidifier and a fixed flow rate, Ntu is inversely proportional to the square of the spacer thickness. (Transfer coefficients and surface area are both inversely proportional to the spacer thickness.) To achieve high system performance, a high dehumidifier Ntu is required. Therefore, a small air gap, probably less than 2 mm (0.08 in.), is desirable. The lower limit of the spacer thickness is determined by practical limitations; because of the relative thickness and surface roughness of the coated ribbon, very thin spacers would tend to produce a nonuniform matrix.

The Australian heat exchangers had an air gap of 0.88 mm (0.035 in.), and this was probably a practical lower limit for a dehumidifier. Preliminary simulations indicated that the Ntu produced with this gap would be quite high and that system performance would not suffer significantly by increasing the gap to 1.5 mm (0.059 in.). Based on these considerations 0.76-mm (0.030-in.) and 1.5-mm (0.059-in.), sheets of high-density polyethylene were obtained and cut into spacers.

When two spacers were inserted between each of the layers, spacings of 2.3 mm (0.091-in.) and 3.0 mm (0.18-in.) could also be studied. Spacings of 1.5 mm and 3.0 mm were used in the four dehumidifiers built for this study.

2.2.5 The Winding Mechanism

A simple mechanism for winding the ribbon onto the hub and spoke assembly with uniform and easily controlled tension was required. Figure 2-5 shows the device that was built for that purpose. Its major parts are the Unistrut® frame, braces for the roll of silica gel ribbon and the hub, and four rollers. The silica gel ribbon unwinds from the roll at the left of the assembly, passes over one roller, then down and around a hanging roller with weights attached to it. From there the ribbon passes over two more rollers and is wound onto the dehumidifier hub. Assuming negligible friction in the rollers, the tension on the ribbon is half the weight of the hanging roller. Each set of spokes is braced during the winding process by a 0.5-in. plexiglass sheet. These sheets also serve as part of a ratchet mechanism used to advance the hub and spoke assembly.

2.3 DEHUMIDIFIER CONSTRUCTION

The different phases of construction of the wound-ribbon dehumidifiers are described in Sections 2.3.1 through 2.3.3. Much of the description is practical advice for those who might want to build similar dehumidifiers and may not be of interest to all readers. The final specifications of the four dehumidifiers are given in Section 2.3.4.

2.3.1 Tape-Coating Procedure

The device shown in Fig. 2-3 was used to coat the double-sided tape with silica gel particles. It was designed to coat both sides at once and to avoid

wasting gel, since the grinding and sieving process is tedious. However, the device worked best when only one side at a time was coated; the paper backing was left on the tape while the first side was coated. The most uniform and dense coating was obtained by simply spreading ample silica gel onto upward-facing tape and brushing off the excess gel.

The mass of the coated tape per unit area and the ratio of silica gel mass to total mass are important input variables for the computer program. Tape rolls were weighed before and after coating, and the length of the tape was measured. Ambient temperature and humidity recorded during the coating process were used to determine the water content of the gel based on the equilibrium data of Rojas [13] for Davison Grade 40 silica gel. The dry mass of the silica gel was calculated from the above. Uncertainties were estimated to be approximately ±3% in the overall dry mass of the ribbon and ±5% in the fraction of silica gel mass to total ribbon mass, based on uncertainties in silica gel equilibrium properties and measured humidity.

2.3.2 Winding Procedure

The device shown in Fig. 2-5 was used to tension-wind the dehumidifiers. To establish a reasonable winding tension, several tests were performed on samples of the coated ribbon. At room temperature, the tape had a tensile strength of about 2.1 kg/cm (12 lb/in.) above which continuous deformation occurred. A tensile load of 0.71 kg/cm (4 lb/in.) was supported by the tape for several hours at room temperature without measurable stretching. However, the same load at 95°C caused considerable stretching. A 0.14-kg/cm (0.80-lb/in.) load caused no observable stretching over four days at 95°C, and this was used as a rough guideline for tension during the first winding attempt.

The dehumidifier hub and the spool of desiccant ribbon were mounted onto the winding frame, and adjustments were made to align the axes of the hub, spool, and rollers to be level and parallel. The ribbon was threaded through the rollers and anchored to the slot in the hub with an aluminum bar and four screws. Tension was applied by adding weights to the pulley assembly. A ratchet mechanism was used to advance the hub and spoke assembly one-eighth of a revolution at a time, and a spacer was inserted manually with each advance (see Fig. 2-6). Care was taken to ensure that the ribbon was correctly aligned as it fed onto the dehumidifier frame. A small shift in the ribbon position tended to be amplified in subsequent revolutions, causing uneven tension and slack areas in the ribbon. Spacers with double-sided tape on each side were used in the last revolution to secure the ribbon. The final length of the ribbon was determined from marks at 1-ft intervals on the ribbon's edge.

According to Ref. [8], the Australian heat exchangers were wound with constant tension. Thus, constant tension was used in our first winding attempt. Ribbon spacing in the resulting dehumidifier, shown in Fig. 2-7, was not as uniform as we would have liked because the inner layers were compressed during the winding process by pressure from successive outer layers. The non-uniformity of the air gaps became considerably worse after only a few absorption tests. Therefore, the dehumidifier was dismantled and rewound using

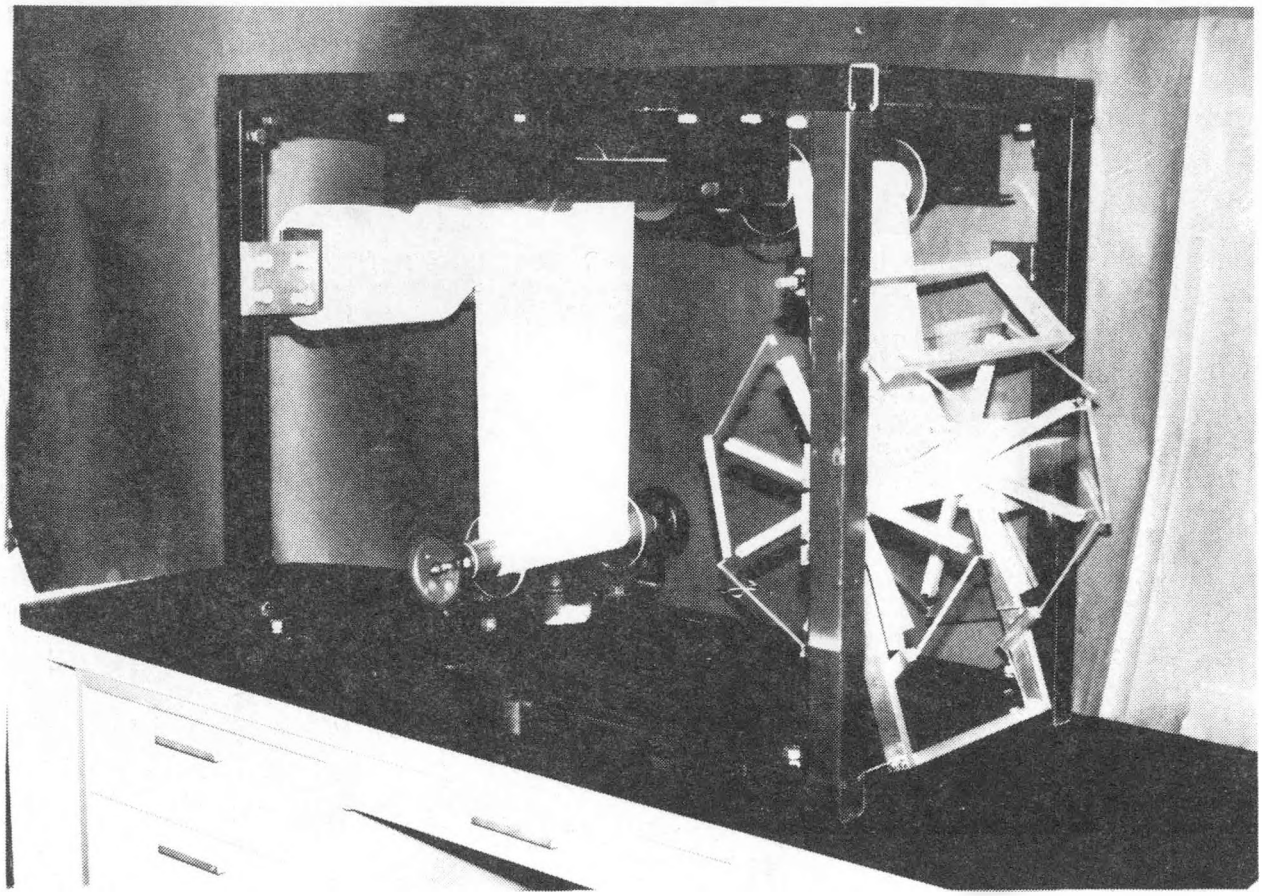

Figure 2-5. Winding Mechanism

constant torque rather than constant tension. This method was suggested by Julian van Leersum of CSIRO, and it worked very well. A tray was attached to the hanging roller of the winding mechanism. Small weights were removed from the tray with the completion of each revolution to maintain roughly constant torque. The final tension was 1.8 kg, somewhat less than that used in the first winding. The uniformity of the dehumidifiers wound in this manner was excellent, allowing us to see through all the passages clearly.

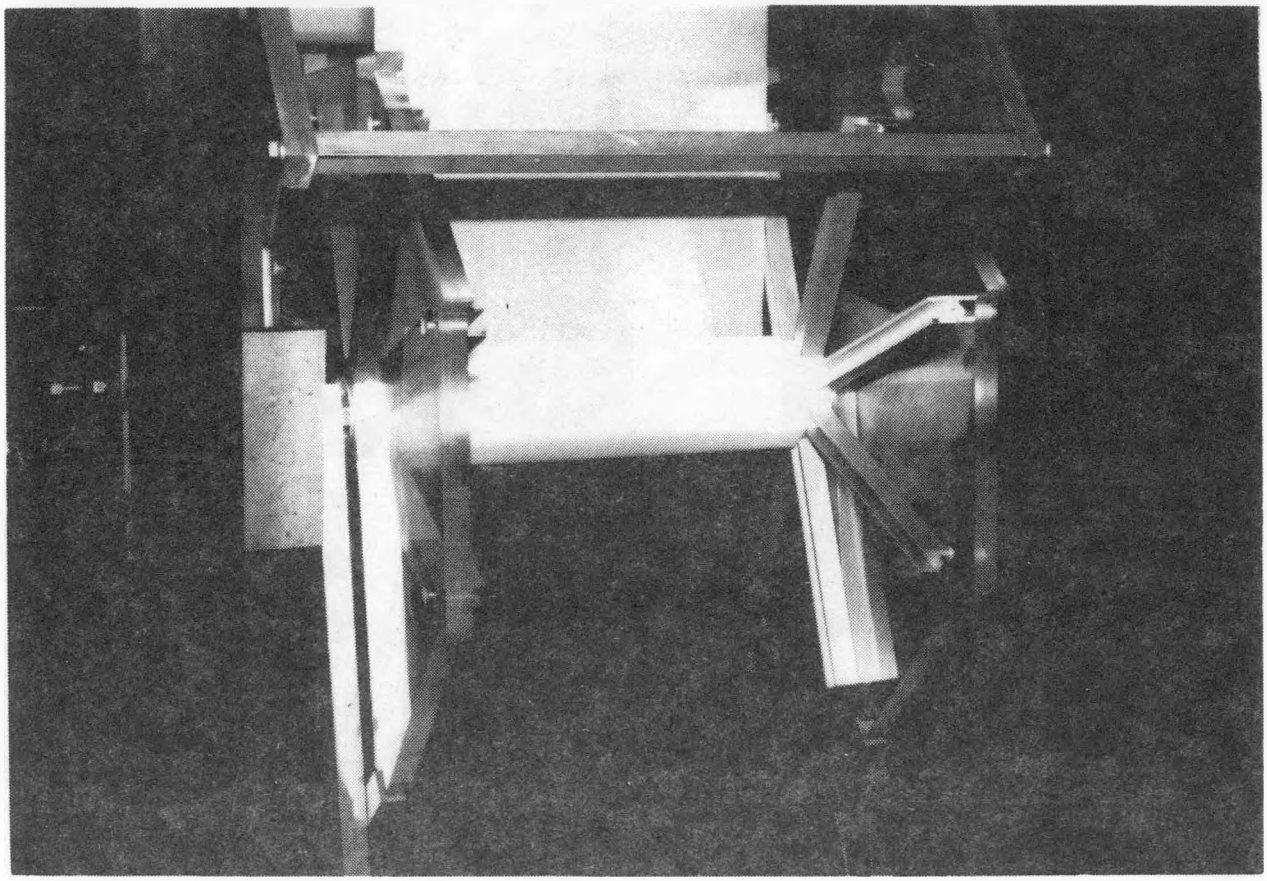

Figure 2-6. Placement of Spacers during Winding

2.3.3 Assembly of the Dehumidifier Module

The first dehumidifier is shown fully assembled in Fig. 2-8. Aluminum sheets were attached to each of the eight sides of the dehumidifier shown in Fig. 2-7 using double-sided tape to ensure that the outermost ribbon layer would be rigid. The metal jacket around the dehumidifier consisted of a 43-cm (17-in.) long, 24-gauge standard connector for 12-in. spiral duct. The air gaps around the outside of the wound-ribbon matrix were blocked with foam rubber covered by a layer of RTV silicon sealer. The center hub and spoke fairings were made of balsa and were obtained from a hobby shop. These were intended to smooth the streamlines of air entering the dehumidifier and were mounted on each end with double-sided tape.

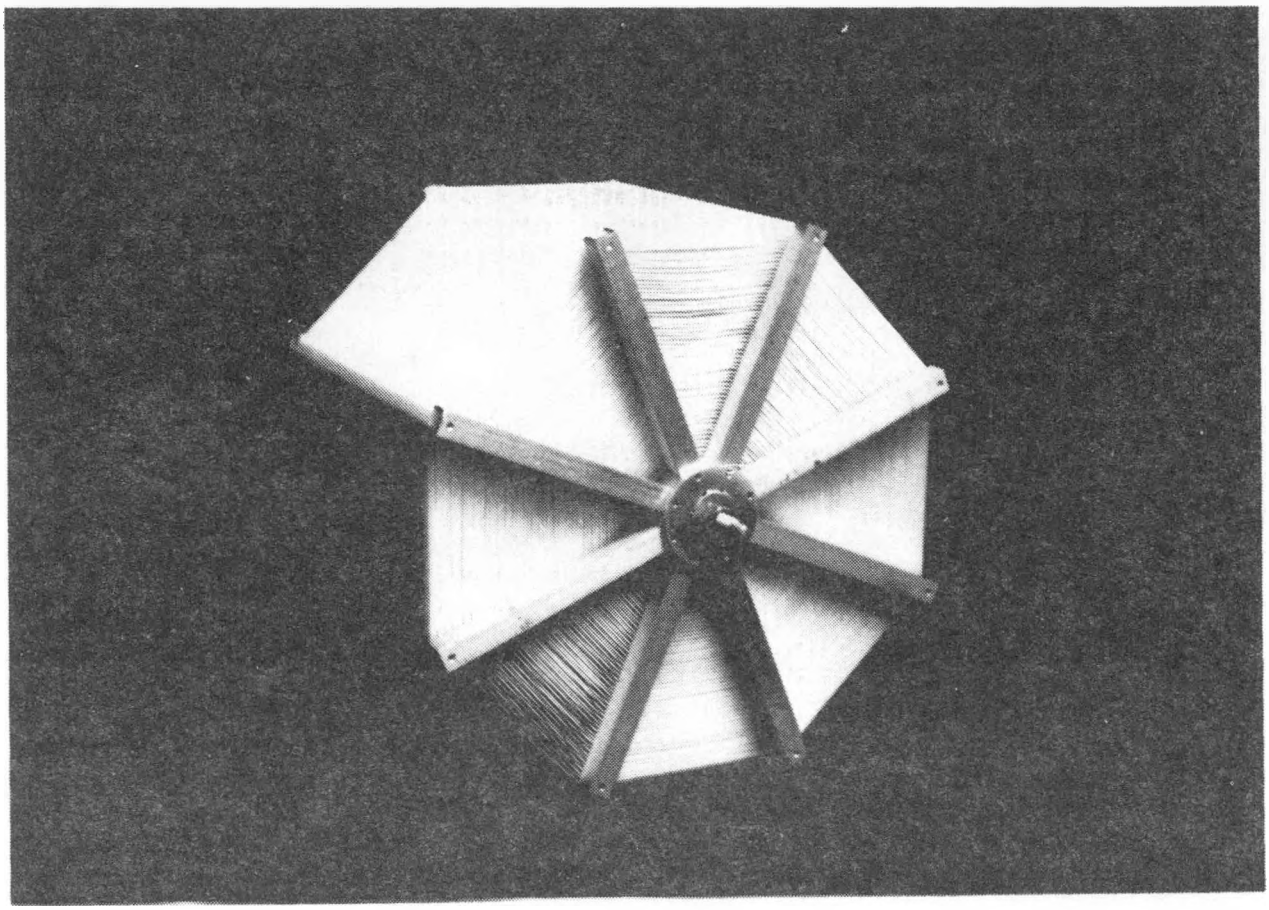

Figure 2-7. Dehumidifier after Winding Process

2.3.4 Dehumidifier Specifications

Once the first dehumidifier was successfully built and tested, an aggressive schedule was adopted to build and test three additional dehumidifiers of different particle size and ribbon spacing. The final specifications of the four dehumidifiers are given in Table 2-2.

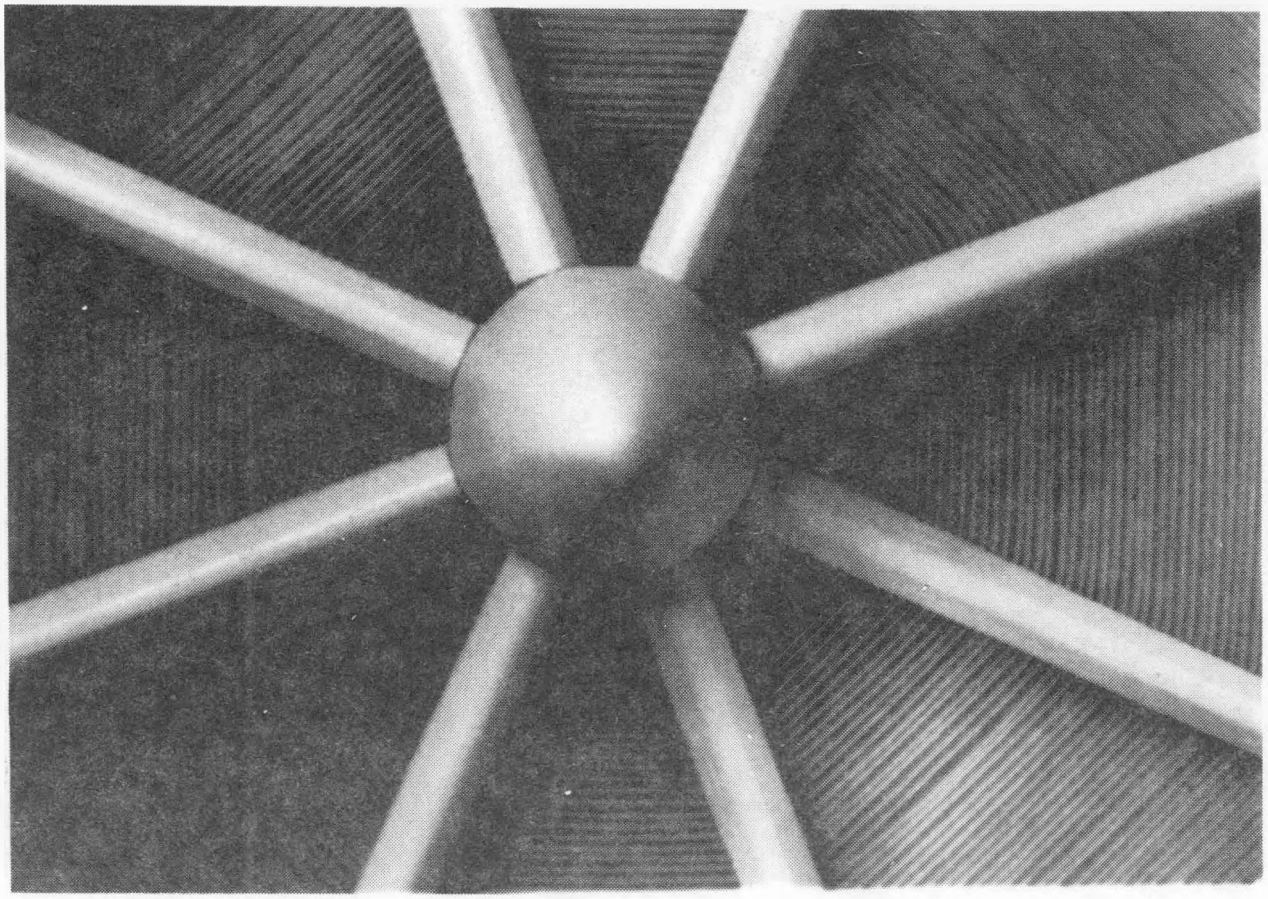

Figure 2-8. Fully Assembled Parallel-Passage Dehumidifier

Table 2-2. Dehumidifier Prototype Specifications

General specifications

Diameter:	0.31 m
Length:	0.20 m
Frontal area:	0.073 m^2
Tape:	Mystik 6466 polyester tape
Desiccant:	Davison Type 40 microporous silica gel

Test specifications

Prototype	Particle Size		Wt. Fraction Silica Gel	Passage Spacing (mm)	Sheet Thickness (mm)
	Min. (mm)	Max. (mm)			
A	0.180	0.250	0.62	1.32	0.58
B	0.355	0.500	0.79	1.42	1.09
C	0.180	0.250	0.62	2.78	0.58
D	0.355	0.500	0.79	2.71	1.09

SECTION 3.0

EXPERIMENTAL APPARATUS AND PROCEDURE

3.1 DESICCANT TEST LOOP

The desiccant test loop was designed by Chuck Kutscher (SERI) to conduct single-blow absorption/desorption tests on desiccant beds. Before the current study it was used to investigate the performance of packed-bed dehumidifiers as reported in Ref. [7] (see that report for a detailed description of the facility). Only minor modifications of the loop were required to test the wound-ribbon dehumidifier, and these modifications are described below along with a brief review of the layout of the test loop.

Figure 3-1 is a schematic of the desiccant test loop showing the location of major components and measurement points. Components for controlling inlet air conditions are (1) a 35-kW_e duct heater, (2) a 6-kW_e duct heater, and (3) a 50-kW_e boiler. These units were originally designed to condition air at a 0.17-kg/s (300 scfm) flow rate, six times the nominal flow rate used in the current experiments. However, existing control equipment allowed power to be controlled down to the low levels needed. The only modification required was the installation of a 1/4-in. valve in the steam line for manual control of the steam injection rate.

The test section was modified to incorporate new instrumentation and to accept the new dehumidifier. Three-inch sections of 1/4-in. cell fiberglass honeycomb were installed on each side of the test section for flow straightening. Two layers of 3-in. fiberglass insulation were used between the two flow nozzles to reduce temperature gradients between duct walls and the air stream in the test section to reduce errors due to radiation effects. The rest of the loop is insulated with a single layer of fiberglass.

3.2 INSTRUMENTATION

Important quantities to measure in these experiments are inlet and outlet temperatures and humidities, flow rate, and pressure drop through the dehumidifier. Temperatures were measured using type T (copper-constantan) thermocouples. Humidities were measured using two General Eastern 1100DP dew point hygrometers. ASTM 2.5-in. nozzles were used for flow measurements; pressure drops were sensed by MKS Model 221 capacitance-type pressure transducers.

Figure 3-2 is a photograph of the test section showing the locations of the dew point hygrometers and pressure transducers as well as the overall arrangement of the test section and dampers. Hygrometers were mounted as close to the sampling points as possible to minimize the time required for air to pass through the sampling lines.

Figure 3-3 shows the arrangement of the thermocouple array and hygrometer intake manifold within the test section. (Identical arrangements are on each side). The eight thermocouples in the array are in horizontal and vertical lines with two junctions in each quadrant. The hygrometer manifold is in the

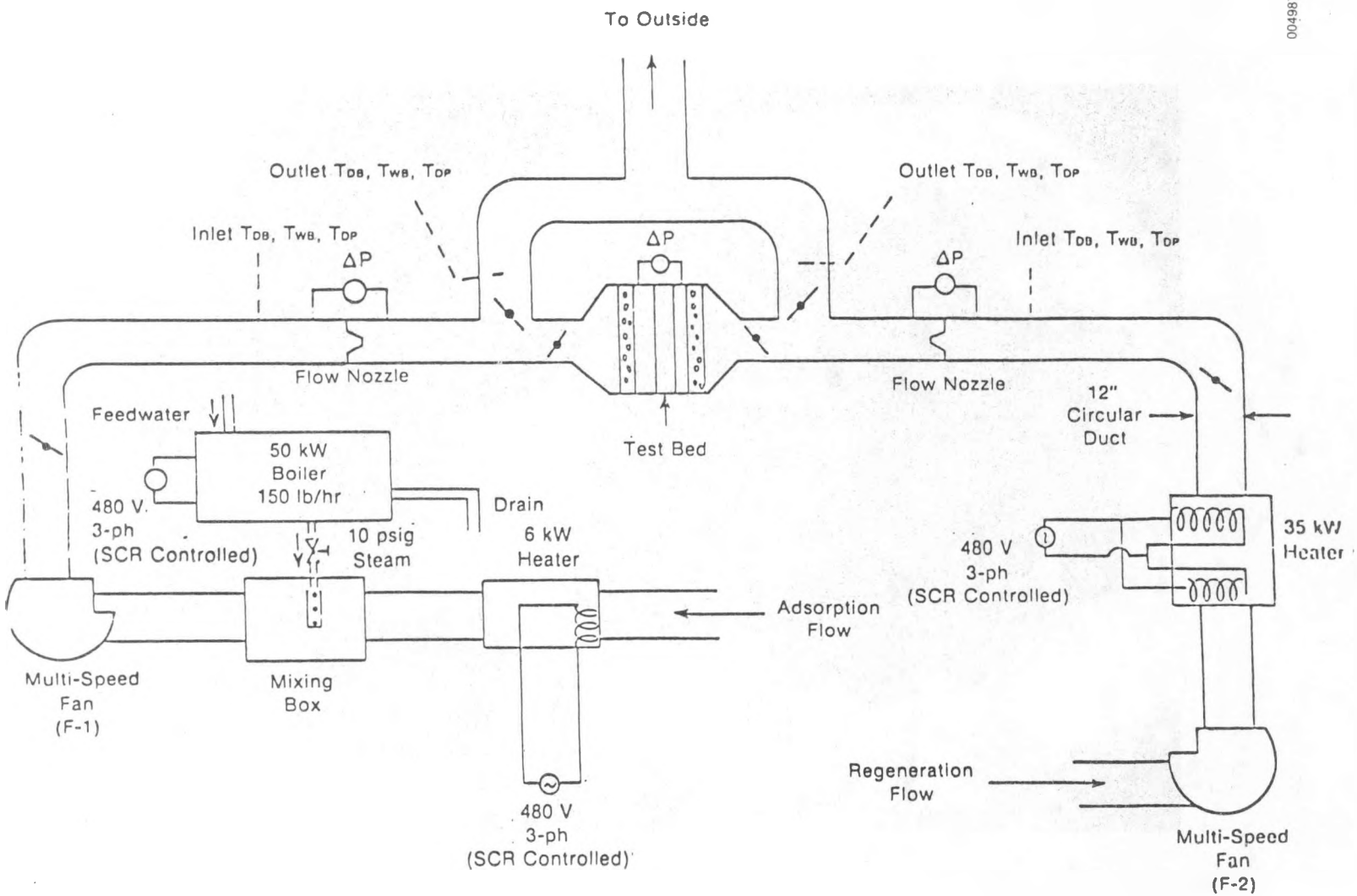

Figure 3-1. Schematic of SERI Desiccant Test Loop

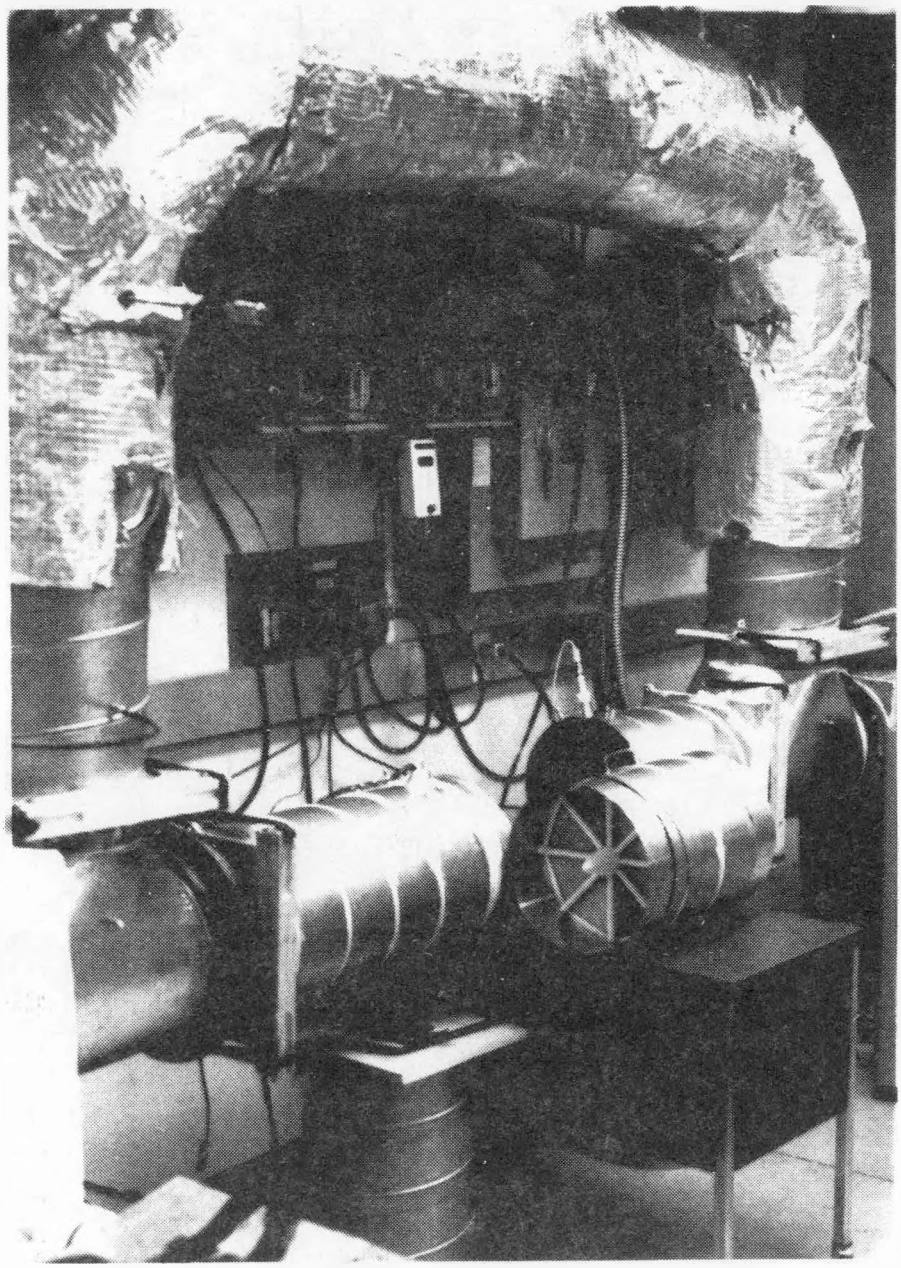

Figure 3-2. Dehumidifier Test Section and Instrumentation

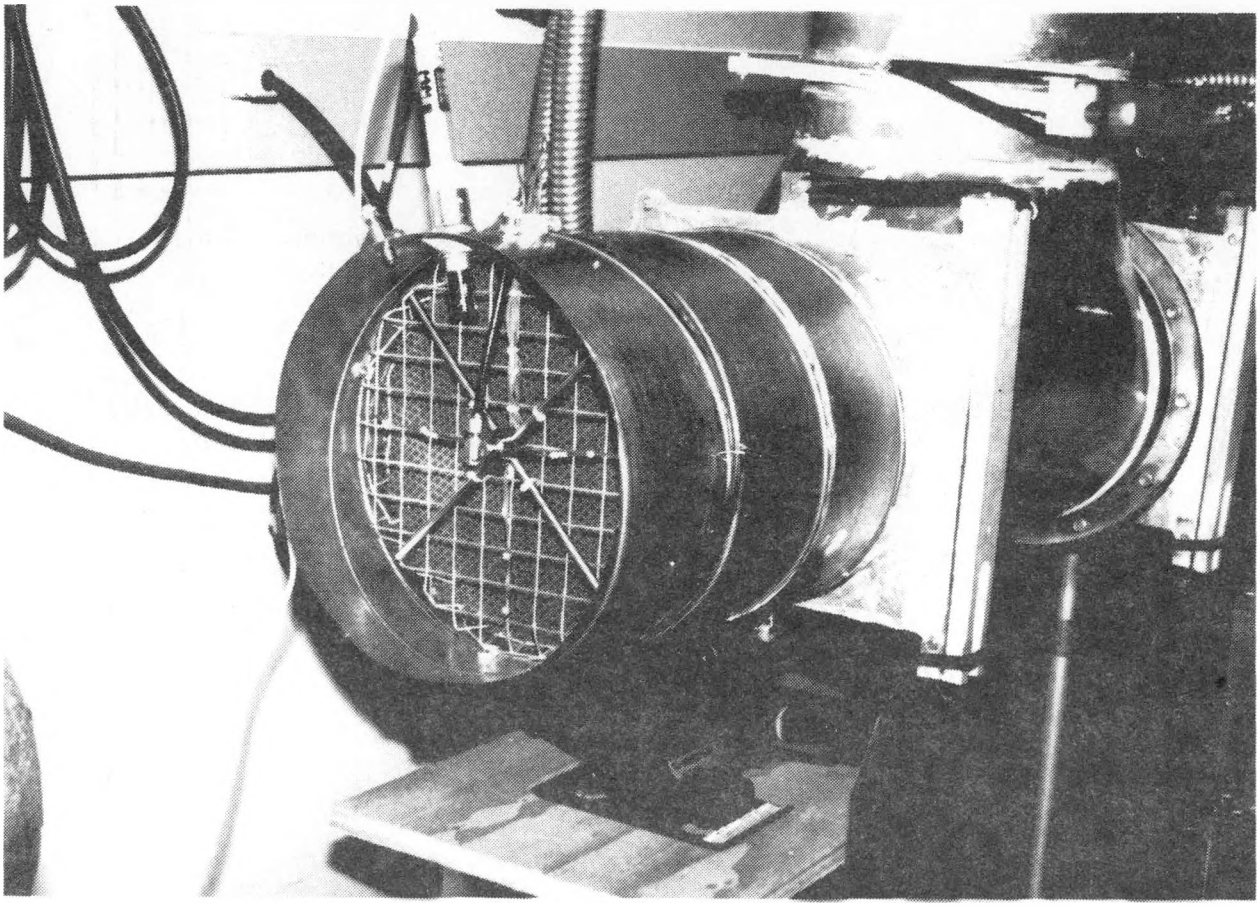

Figure 3-3. Thermocouple Array and Hygrometer Intake Manifold in Test Section

shape of a cross at a 45-degree angle to the thermocouple array. This arrangement aligns with the eight pie-shaped sections of the wound-ribbon dehumidifier as shown in Fig. 3-4, so as to measure the average outlet temperature and humidity from the uniform parallel-walled matrix while minimizing the influence of the outside wall, the spacers, and the hub. This allows direct comparison of measured results with computer predictions, since the computer model does not include these boundary effects.

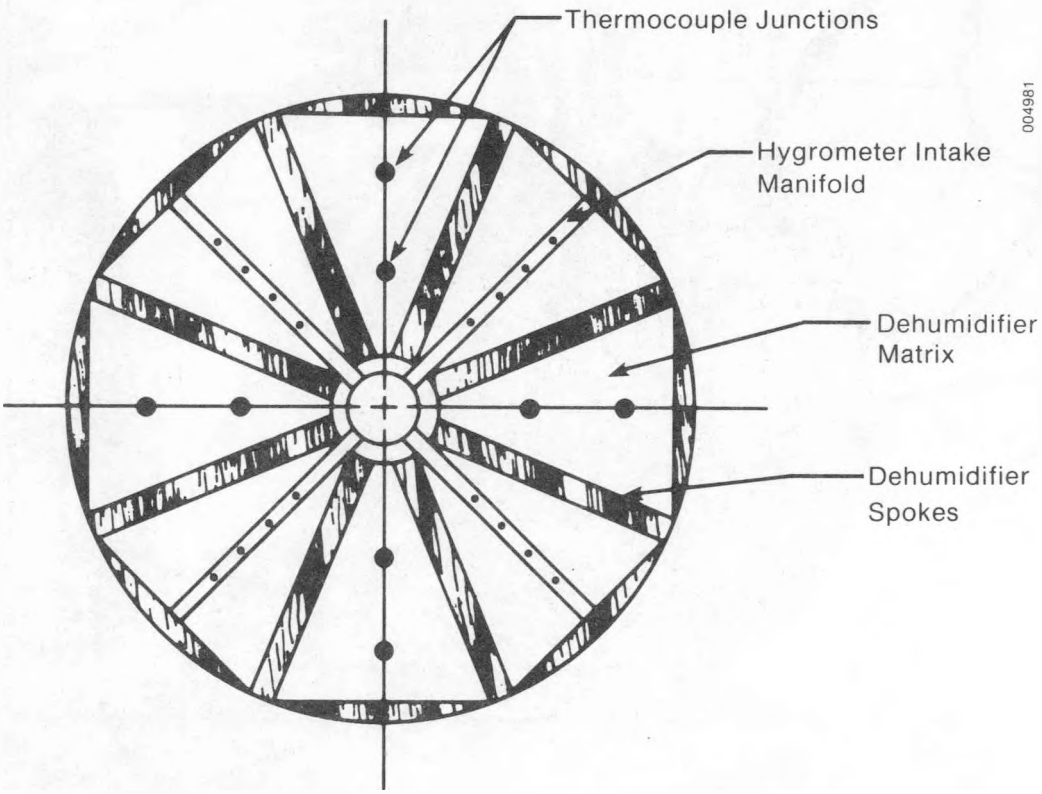

Figure 3-4. Spatial Arrangement of Temperature and Humidity Sensors in Test Section

3.3 DATA ACQUISITION

The data acquisition system used in these experiments is shown in Fig. 3-5. It consists of a Hewlett-Packard HP-85 microcomputer, an HP 3497A Data Acquisition/Control Unit, an HP 7225B single-pen plotter, and an Epson MX-80 dot matrix printer. Software was written to automatically scan all channels every 30 seconds, reduce raw data, and print and plot results on a continuous basis. Real-time plotting of results was particularly useful.

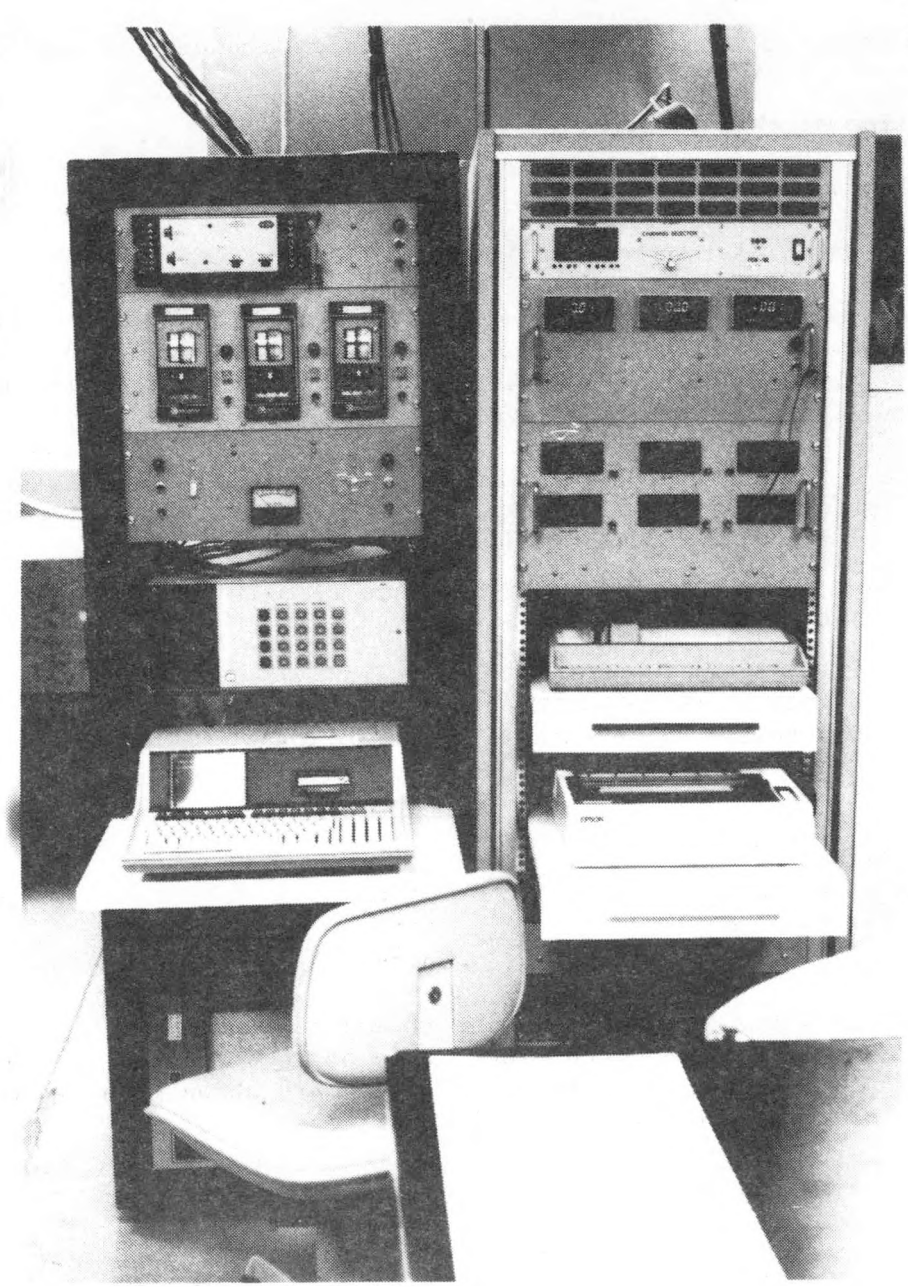

Figure 3-5. Data Acquisition System

3.4 QUALIFICATION PROCEDURES

Several tests were performed on the facility to qualify it before the wound-ribbon dehumidifier was tested. These included the following:

- Measurement of damper leakage rates to allow correction of flow rates
- Measurement of vertical and horizontal temperature and humidity profiles in the test section
- Determination of the stability of inlet conditions (temperature, humidity, flow rate)
- Calibration of the dew-point hygrometers.

Results are summarized below.

- Damper leakage was measured by installing a flow nozzle in the test section; identical nozzles were located upstream and downstream of the damper being tested. Measurements were taken and compared over a range of flow rates first with the damper completely sealed with putty, then with the damper in its normal closed position. Damper leakage was found to be roughly linear with pressure drop across the damper over the range of pressure drops encountered. During experiments the pressure drop across the bypass damper upstream of the dehumidifier was measured and the flow rate through the dehumidifier was corrected accordingly. Leakage rates were typically 1.5% to 3% of the total flow rate.
- Inlet humidity is uniform across the duct to within 0.0002 kg/kg, within the noise level of the hygrometer.
- Inlet temperature profiles are relatively flat across the 9- or 10-inch core of the duct where measurements are made. Variations across the core for several conditions are summarized as follows:

Flow Rate	Average Temperature	Core Uniformity
0.028 kg/s (50 scfm)	35°C	±0.1°C
0.051 kg/s (90 scfm)	35°C	±0.1°C
0.028 kg/s (50 scfm)	80°C	±0.5°C
0.051 kg/s (90 scfm)	80°C	±0.3°C

- Inlet humidity was generally stable to within ±0.0005 kg/kg with random fluctuations of humidity occurring for no obvious reason. These fluctuations and their effect on outlet conditions are shown clearly in the data and do not detract from its overall usefulness.
- As a rule, very stable inlet temperatures could be achieved with a slow drift of 1° to 2°C occurring in some runs.
- Dew-point hygrometers were calibrated by comparing dew-point readings with thermocouple readings for saturated air over a range of temperatures. Saturated air was obtained by drawing air through a 20-ft copper tube containing a damp wick. The copper tube was coiled up and placed in an insulated, vigorously stirred water bath. Results are given in Fig. 3-6. Hygrometers are shown to be accurate to within ±0.4°C over the range of dew-point temperatures of interest in these experiments.

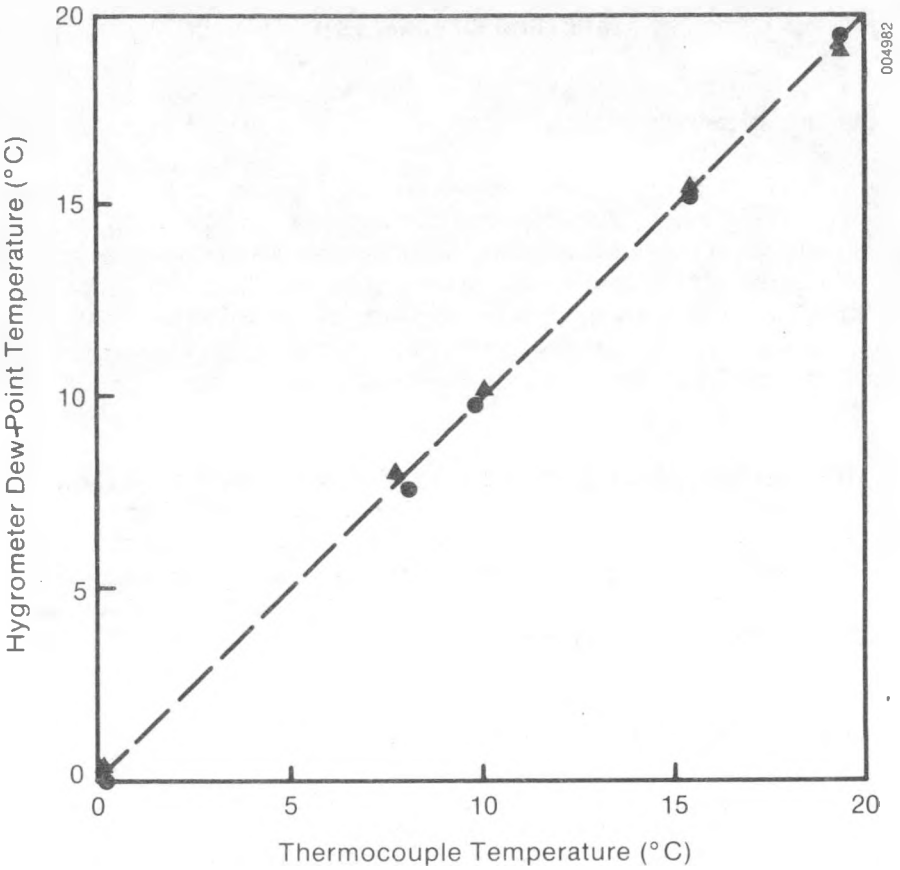

Figure 3-6. Hygrometer Calibration Results

SECTION 4.0

METHOD OF ANALYSIS

4.1 REVIEW OF THE COMPUTER MODEL

A computer model for predicting the heat and mass transfer performance of silica gel desiccant beds (DESSIM) is documented in Ref. [5]. The equations for simple, steady-state, counterflow heat exchangers and mass exchangers are used within a finite-difference calculation procedure to generate a pseudo-steady-state model. The use of these equations simplifies the mathematics of the absorption analysis, yet allows the use of relatively large time and space increments and makes the model easy to adapt to a variety of drying situations.

The DESSIM model was originally developed for the investigation of packed-bed dehumidifiers. Three versions of the program were written: one for single-blow predictions, one for desiccant cooling system performance predictions, and one for parametric investigations of system performance. All three versions were modified to treat the wound-ribbon dehumidifier geometry based on the analysis in the next section.

4.2 ANALYSIS OF THE WOUND-RIBBON DEHUMIDIFIER

In this investigation, the wound-ribbon dehumidifier is treated as a uniform matrix of parallel-walled channels. Effects of support materials (hub, spacers, and spokes) and the outer wall of the dehumidifier are not included in the analysis. Although it would be desirable to include these effects, it would be very difficult to do so accurately. Data from a rotating dehumidifier of larger scale will be needed to evaluate the effects of this additional inert thermal mass in the dehumidifier.

Additional assumptions used in the model are as follows:

- Flow is laminar and fully developed.
- There is no temperature gradient across the ribbon; i.e., heat transfer is convectively controlled.
- The effect of the resistance to moisture diffusion within the silica gel particles can be adequately accounted for through the use of a lumped gas-side mass transfer coefficient.
- Axial conduction, diffusion, and dispersion are negligible.
- Silica gel particles act as a uniform, flat coating on the substrate.

Under these assumptions the analysis of the wound-ribbon geometry is relatively simple, having fewer ambiguities than the analysis of packed beds. The dry mass of the ribbon, the fraction that is silica gel, the thickness of the ribbon, and its spacing within the finished matrix can all be measured. From these measurements the information needed for the pseudo-steady-state calculation can be obtained. Figure 4-1 shows the geometry of interest:

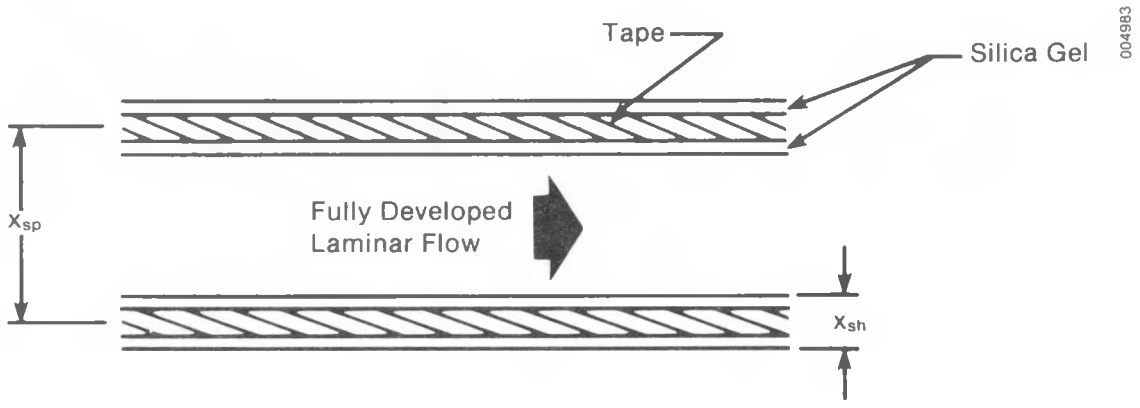

Figure 4-1. Parallel-Passage Geometry

x_{sh} is the thickness of the ribbon and x_{sp} is the center-to-center spacing of the ribbons. The number of ribbon sheets per unit height of the matrix is $(1/x_{sp})$. Thus, the surface area per unit volume is

$$A = 2/x_{sp} \quad . \tag{4-1}$$

The hydraulic diameter of each channel is equal to twice the air gap:

$$d_h = 2(x_{sp} - x_{sh}) \quad . \tag{4-2}$$

If the dry mass of the sheet per unit area is M_{sh}, then the density of the matrix is

$$\rho_b = M_{sh}/x_{sp} \quad . \tag{4-3}$$

If F is the mass fraction of silica gel on the ribbon and c_g and c_p are specific heats for the gel and the plastic substrate, then the specific heat of the overall dry matrix is

$$C_b = F_{cg} + (1-F)c_p \quad . \tag{4-4}$$

Heat transfer Nusselt numbers for fully developed laminar flow between infinite parallel plates can be calculated theoretically for the cases of constant wall temperature (Nu = 7.5) and constant heat flux (Nu = 8.4). Adsorption does not fit either of these limits, but the conservative value of 7.5 is used here.

The heat transfer coefficient is then

$$h = kNu/d_h, \quad Nu = 7.5 \ , \tag{4-5}$$

where k is the conductivity of air. The mass transfer coefficient is calculated from h and an effective Lewis number that accounts approximately for the resistance to moisture diffusion within the silica gel particles

$$g = h/(Le_{eff}c_a) \ . \tag{4-6}$$

Here, c_a is the specific heat of air. The effective Lewis number for typical packed-bed dehumidifiers has been found to be about 3 [3,7]. Scientists at UCLA have estimated the effective Lewis number to be approximately 1.2 for their parallel-plate dehumidifier. Previous experience has shown that small changes in the Lewis number have little effect on single-blow predictions. Therefore, the value Le = 1.2 was used initially in this study. Equations 4-1 through 4-6 are all that are needed to modify the pseudo-steady-state model for heat and mass transfer to treat the wound-ribbon geometry.

In the new programs, pressure drop through the dehumidifier is predicted based on the assumption of fully developed laminar flow

$$\Delta P = \frac{\rho V^2}{2g_c}\left[K_c + K_e + 4f\frac{L}{D}\right] \ , \quad f = \frac{24}{Re} \ . \tag{4-7}$$

K_c and K_e are contraction and expansion coefficients that make only minor contributions. Equations based on data from Ref. [16] for these coefficients are

$$K_c = 0.8 - 0.1\sigma - 0.2\sigma^2 \ ,$$

and

$$K_e = 1.0 - 2.4\sigma + \sigma^2 \ , \tag{4-8}$$

where

$$\sigma = (x_{sp} - x_{sh})/x_{sp} \ .$$

4.3 MODIFICATION OF THE COMPUTER MODEL

As indicated in the previous section, few changes in the computer programs were necessary for analysis of the wound ribbon dehumidifier. Complete listings of the DESSIM programs for packed beds are given in Ref. [5]. Table 4-1 gives definitions of new FORTRAN variables.

Table 4-1. New FORTRAN Variables for the Wound-Ribbon Simulation Programs

FORTRAN Variable	Text Variable	Definition
CGEL	c_g	Specific heat of silica gel (J/kg ^oC)
CPLAST	C_p	Specific heat of plastic ribbon (J/kg ^oC)
DELTAP	ΔP	Predicted pressure drop (N/m^2)
DH	D_h	Hydraulic diameter of passages (m)
DPH2O		Predicted pressure drop ("H_2O)
RE	R_e	Reynolds number
RKC	K_c	Contraction coefficient in pressure drop calculation
RKE	K_e	Expansion coefficient in pressure drop calculation
RNUSLT	Nu	Nusselt number
SHMASS	M_{sh}	Dry mass of coated ribbon (kg/m^2)
SIGMA	σ	Used in pressure drop calculation (like void fraction)
VEL	V	Velocity of air within the dehumidifier (m/s)
XSHEET	X_{sh}	Thickness of coated ribbon (m)
XSPACE	X_{sp}	Center-to-center spacing of ribbon layers in the dehumidifier (m)

SECTION 5.0

RESULTS

5.1 SUMMARY OF RUNS

A total of 24 single-blow adsorption and desorption runs were completed on four wound ribbon dehumidifiers. Conditions for these runs are summarized in Table 5-1, and specifications of the dehumidifiers were given in Table 2-2. The first dehumidifier was subjected to the most complete set of tests, covering a range of conditions representative of desiccant cooling system operation and including pressure drop data over a wide range of flow rates. Tests on the three additional dehumidifiers were performed to obtain data on the effects of ribbon spacing and desiccant particle size. Figure 5-1 shows the inlet conditions for each test on a psychrometric chart.

5.2 GRAPHIC COMPARISON OF EXPERIMENTAL DATA AND PREDICTIONS

Measured and predicted results for each run are plotted together in the Appendix. Experimental data were plotted during the actual runs and later superimposed on the plot of predicted results. Inlet and outlet conditions are shown for both measured data and predictions, allowing a clear representation of the effects of fluctuations and drift in the inlet air conditions.

In reviewing the graphic comparisons in the Appendix, the reader should consider that

- Humidity data taken during the first one to three minutes of each run are of questionable accuracy because of the slow response rate of the dew-point hygrometers compared with the rapid transient in outlet humidity during this time.
- The dew-point hygrometers have a ramp rate of $3^{o}C/s$, which is ample for tracking the outlet humidity after its initial rapid change.
- The low initial inlet air temperature is observed in several of the regeneration runs because the metal duct in the test section cools to some extent while the dehumidifier is being installed and the regeneration air is being bypassed.

The graphic comparisons in the Appendix represent the validation of the DESSIM model with respect to experimental results. Since this forms the basis for projected performance of the dehumidifier design in desiccant cooling system operation, the agreement of the simulation results and test results deserves attention.

Both adsorption and regeneration experiments have breakthrough curves that are flatter than those predicted by the simulation. Transient peaks associated with temperature and humidity waves are also less pronounced than anticipated. This behavior is probably caused by heat loss and capacitance

Table 5-1. Summary of Runs

Run No.	Date (1982)	Run[a] Type	Inlet Conditions: Temp. (°C)	Inlet Conditions: Humidity (kg/kg)	Inlet Conditions: Air Flow (kg/s)	Predicted Bed Water Content: Initial (kg/kg)	Predicted Bed Water Content: Final (kg/kg)	Reynolds Number	Pressure Drop: Measured (N/m^2)	Pressure Drop: Predicted (N/m^2)
Type A										
1	7-12	R	70.3	0.0100	0.0280	0.1835[b]	0.0253	101	17.8	26.9
2	7-13	A	35.6	0.0178	0.0283	0.0253	0.2066	109	21.0	22.3
3	7-13	R	80.6	0.0119	0.0276	0.2066	0.0189	96	20.7	27.5
4	7-14	A	40.5	0.0139	0.0292	0.0189	0.1283	111	20.5	23.7
5	7-14	R	85.3	0.0098	0.0292	0.1283	0.0136	101	21.9	29.7
6	7-15	A	34.6	0.0099	0.0287	0.0136	0.1312	111	21.1	22.5
7	7-15	R	70.4	0.0140	0.0282	0.1312	0.0325	101	18.9	26.7
8	7-16	A	30.4	0.0140	0.0283	0.0325	0.2235	110	21.2	21.7
9	7-16	R	79.8	0.0100	0.0281	0.2235	0.0171	98	20.6	27.9
10	7-19	A	34.8	0.0140	0.0282	0.0171	0.1753	109	21.6	22.1
11	7-19	R	79.5	0.0100	0.0446	0.1753	0.0173	156	34.0	44.3
12	7-20	A	35.3	0.0138	0.0508	0.0173	0.1684	196	40.1	40.2
13	7-20	R	82.0	0.0075	0.0443	0.1684	0.0126	154	35.3	44.6
14	7-21	A	35.1	0.0141	0.0283	0.0126	0.1735	109	20.6	22.3
Type B										
15	7-21	R	79.0	0.0100	0.0278	0.2680[b]	0.0177	125	24.2	28.6
16	7-22	A	35.3	0.0138	0.0279	0.0177	0.1684	138	24.9	22.9
17	7-23	R	79.2	0.0102	0.0434	0.1684	0.0178	196	40.0	45.0
18	7-23	A	34.9	0.0137	0.0506	0.0178	0.1710	251	48.9	41.8
Type C										
19	7-26	R	78.9	0.0119	0.0297	0.2200[b]	0.0202	177	5.7	5.3
20	7-27	A	35.4	0.0137	0.0291	0.0202	0.1665	190	5.1	4.2
21	7-28	R	80.0	0.0126	0.0472	0.1526	0.0202	280	9.2	8.6
22	7-28	A	34.8	0.0140	0.0522	0.0202	0.1753	342	9.0	7.5
Type D										
23	7-29	R	79.0	0.0120	0.0294	0.2520[b]	0.0203	197	4.8	6.6
24	7-30	A	36.0	0.0140	0.0290	0.0203	0.1640	214	6.2	5.2

[a] A = adsorption, R = regeneration.

[b] Beds are fully adsorped at ambient conditions for the start of each series; bed water content predicted by DESSIM model.

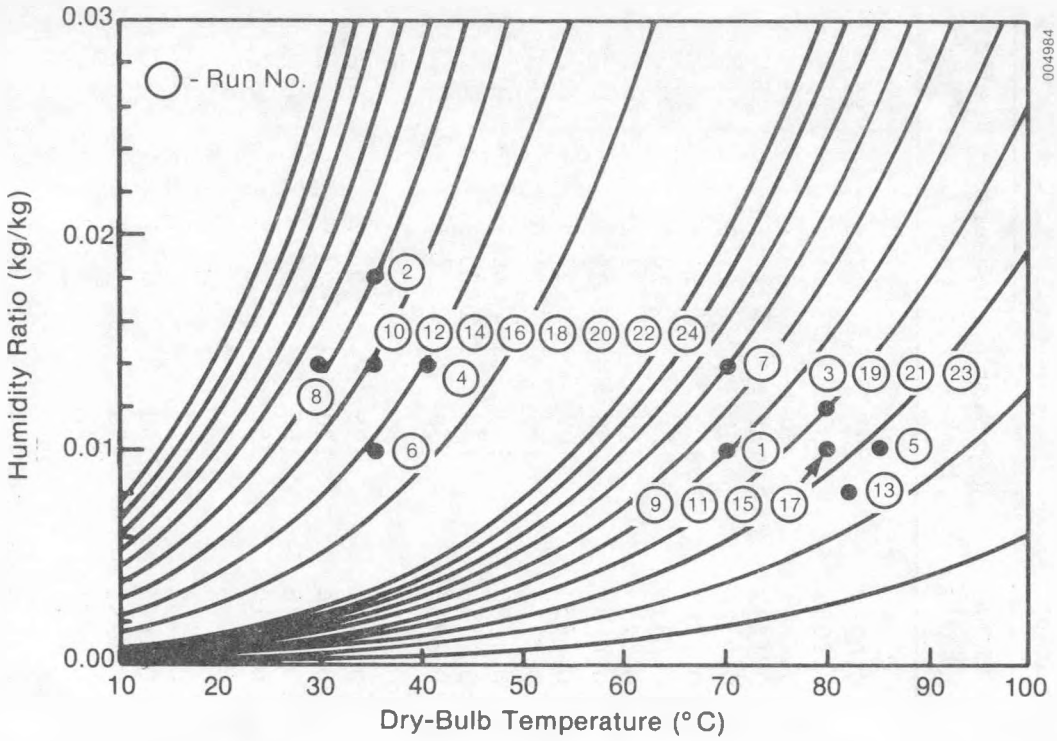

Figure 5-1. Psychrometric Chart of Run Conditions

effects in the experimental apparatus, since steady-state air flow conditions are set up in a bypass loop and then switched to the test bed. Bringing the ductwork and inert parts of the dehumidifier up to air stream temperature will dampen the effects of heat and mass transfer. This explanation is reinforced by the observation that the damping effect lasts longer in regeneration runs where air temperatures are highest and temperature differences greatest. The computer model assumes adiabatic conditions and is not able to account for heat loss/capacitance effects.

There is also a consistent offset in predicting the half-cycle time for the regeneration runs. Typically, the model predicts breakthrough times that are 25%-30% shorter than those observed in the experimental results. Because this effect is seen in regeneration and not in adsorption, it could be attributed to hysteresis effects in the adsorption/desorption cycle. It has been shown that the process path for desorption, or regeneration, is not the same as that for adsorption. The hysteresis in this cycle must be characterized to quantify its effect on system performance predictions.

5.3 PRESSURE DROP RESULTS

The wound-ribbon dehumidifier design was chosen for testing because theoretical analysis showed that it should produce a high ratio of Stanton number to friction factor. This translates, roughly, to a high ratio of performance to pressure drop for a given dehumidifier size and flow rate. Consequently, the pressure drop characteristics of this dehumidifier design were thoroughly tested.

Figure 5-2 shows the pressure drop through the first dehumidifier for a wide range of flow rates that would be of interest in desiccant cooling. Measured pressure drop is in good agreement with the prediction, which is based on the assumption of fully developed laminar flow.

Figure 5-3 shows the correlation of measured and predicted pressure drops for each of the adsorption/desorption test runs.

5.4 DISCUSSION OF EXPERIMENTAL RESULTS

Results of typical runs of the four prototypes with different particle sizes and passage spacings at ARI conditions and 80°C regeneration temperature are summarized in Table 5-2. There is a general trend to increased performance with smaller particles, following from the earlier discussion of smaller solid-side resistance with decreasing particle size. Also, a trade-off is apparent between performance and pressure drop, with changing passage spacing. Smaller passage spacing increases the number of layers in the spiral winding for a given dehumidifier size, increasing the available surface area and inventory of desiccant. This increases the capacity and Ntu for the model with smaller spacing. In contrast, the increased number of layers and small air flow passages increases the pressure drop across the dehumidifier and, subsequently, the fan power required to maintain rated air flows in the system. This trade-off of performance versus pressure drop is an optimization that must be considered in system designs.

Table 5-2. Summary of Experimental Results

Prototype	Particle Size		Passage Spacing (mm)	Effective Ntu		Pressure Drop (Pa)
	Min (mm)	Max (mm)		Adsorption	Desorption	
A	0.180	0.250	1.32	27.1	30.2	20
B	0.355	0.500	1.42	19.1	21.2	25
C	0.180	0.250	2.78	7.3	8.1	5
D	0.355	0.500	2.71	6.6	7.3	6

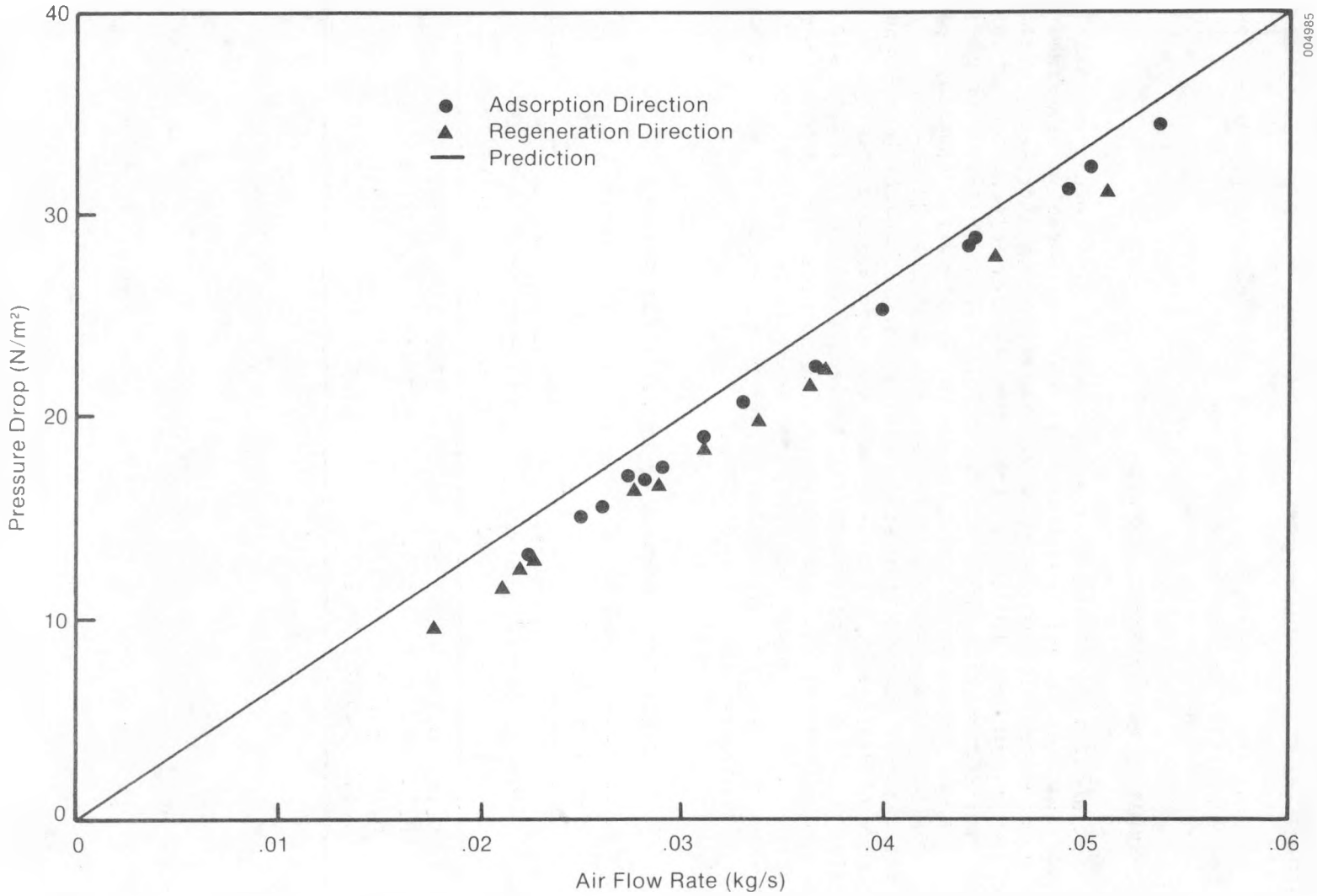

Figure 5-2. Pressure Drop versus Flow Rate—Measured and Predicted

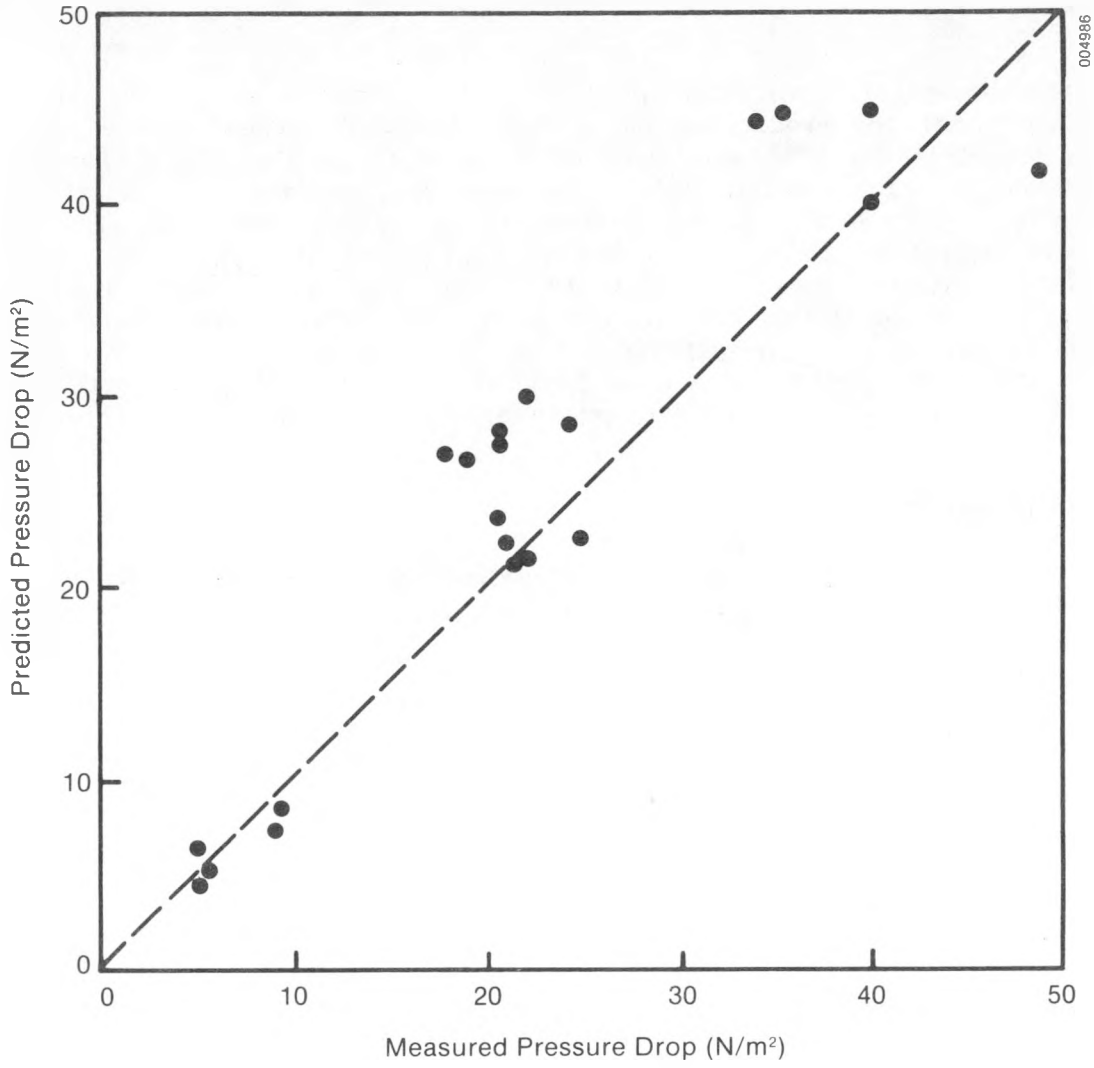

Figure 5-3. Pressure Drop during Experimental Runs

SECTION 6.0

SYSTEM PERFORMANCE STUDIES

The DESSIM computer simulation proved in the experimental phase to be an acceptable model for predicting the single-blow performance of the parallel-passage dehumidifier. The model can now be used to predict the performance of a desiccant cooling system using the new dehumidifier design [10]. To evaluate the effects of various parameters on system performance, a simple model was used that incorporated balanced process air flows, 90% effective evaporative coolers, and a 95% effective heat exchanger. The dehumidifier wheel is 1 m in diameter and 0.20 m in depth, rotating at a speed of 15 revolutions per hour for a half-cycle time of two minutes. Standard ARI conditions are used for indoor and outdoor air states, and a regeneration air state of 80°C, 0.010 kg/kg humidity are used unless otherwise specified.

6.1 DESIGN PARAMETERS

Figure 6-1 presents projected desiccant cooling system performance using parallel-passage dehumidifiers with varying channel spacing and desiccant particle size. In general, thermal COP and electrical COP are improved by the use of small desiccant particles, with no apparent effect in specific capacity. Channel spacing has a marked effect on all three system performance measures. Thermal COP and capacity are markedly improved by close channel spacing, while electrical COP is rapidly degraded as spacing is reduced. This represents the trade-off that must be made between performance and parasitic power in the optimization of system design. Even so, at the smallest channel spacing (0.7 mm) and particle size (0.11 mm) considered, performance levels with thermal COP of 1.07 kw/kw and specific capacity of 16.7 kJ/kg dry air can be matched with an electrical COP of 7.9 kw/kw (27 EER). A system with such a design point would surpass present performance levels for prototype desiccant cooling systems.

6.2 PROCESS VARIABLES

System performance was mapped with respect to variable conditions of room temperature and humidity, ambient conditions, and regeneration temperature. Note that, with design parameters of channel spacing and particle size fixed at 0.7 mm and 0.11 mm, respectively, the parasitic power use will be fixed at a given flow rate. Therefore, electrical COP, the ratio of cooling capacity/power consumption, varies directly with capacity. As shown in Fig. 6-2, room conditions, or the constraints on the state of the air delivered by the system, have a small effect on all performance factors. Comfort-zone limits that allow the delivered air to be warmer and/or more humid will increase performance. Ambient conditions, as seen in Fig. 6-3, have strong effects on specific capacity and electrical COP, while thermal COP is affected only by a combination of high temperature and high humidity. This characteristic of the thermal COP is primarily a result of the use of high-effectiveness heat exchangers and dehumidifiers that tend to insulate the system from changes in air supply conditions. Only when the enthalpy of the air goes above the

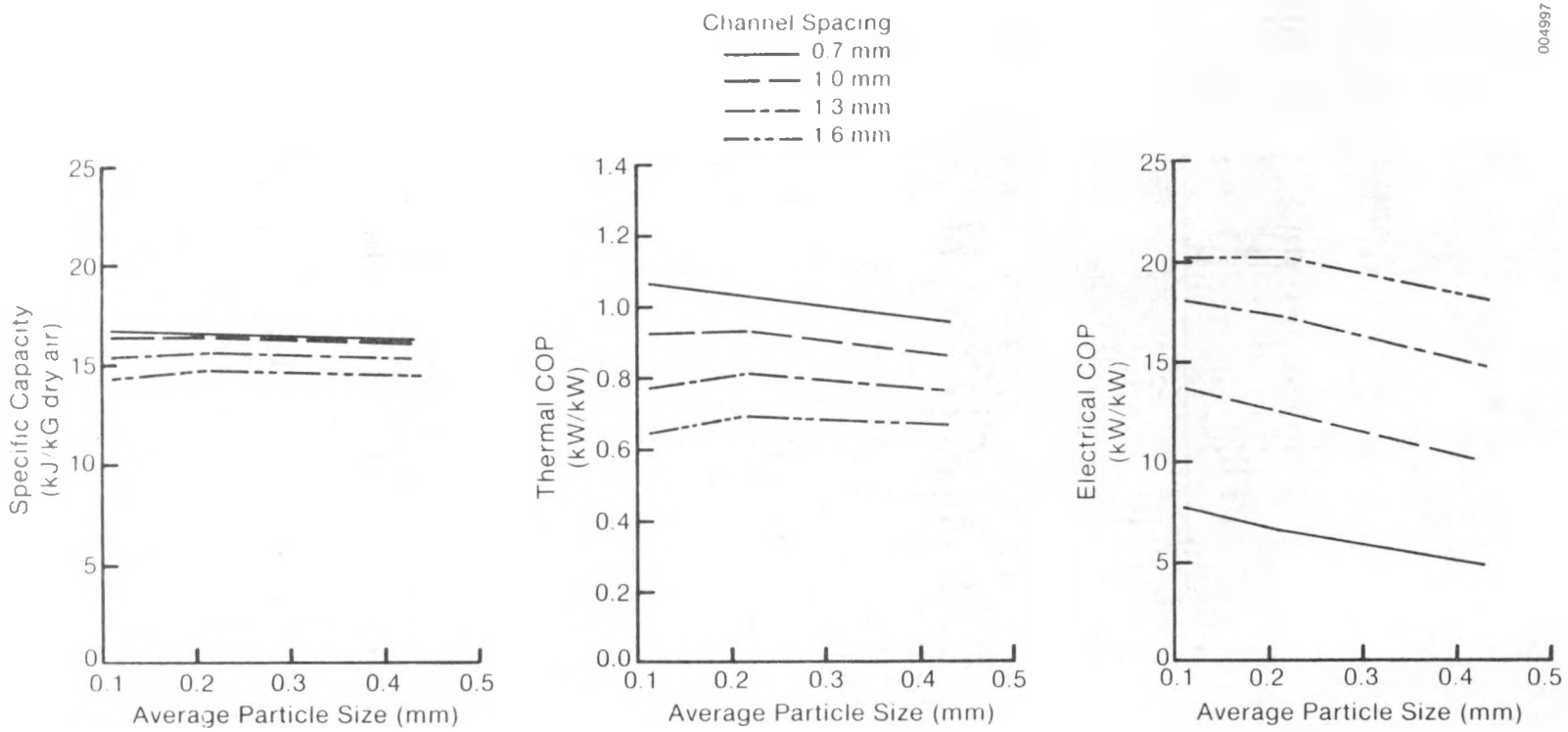

Figure 6-1. System Performance versus Desiccant Particle Size and Channel Spacing

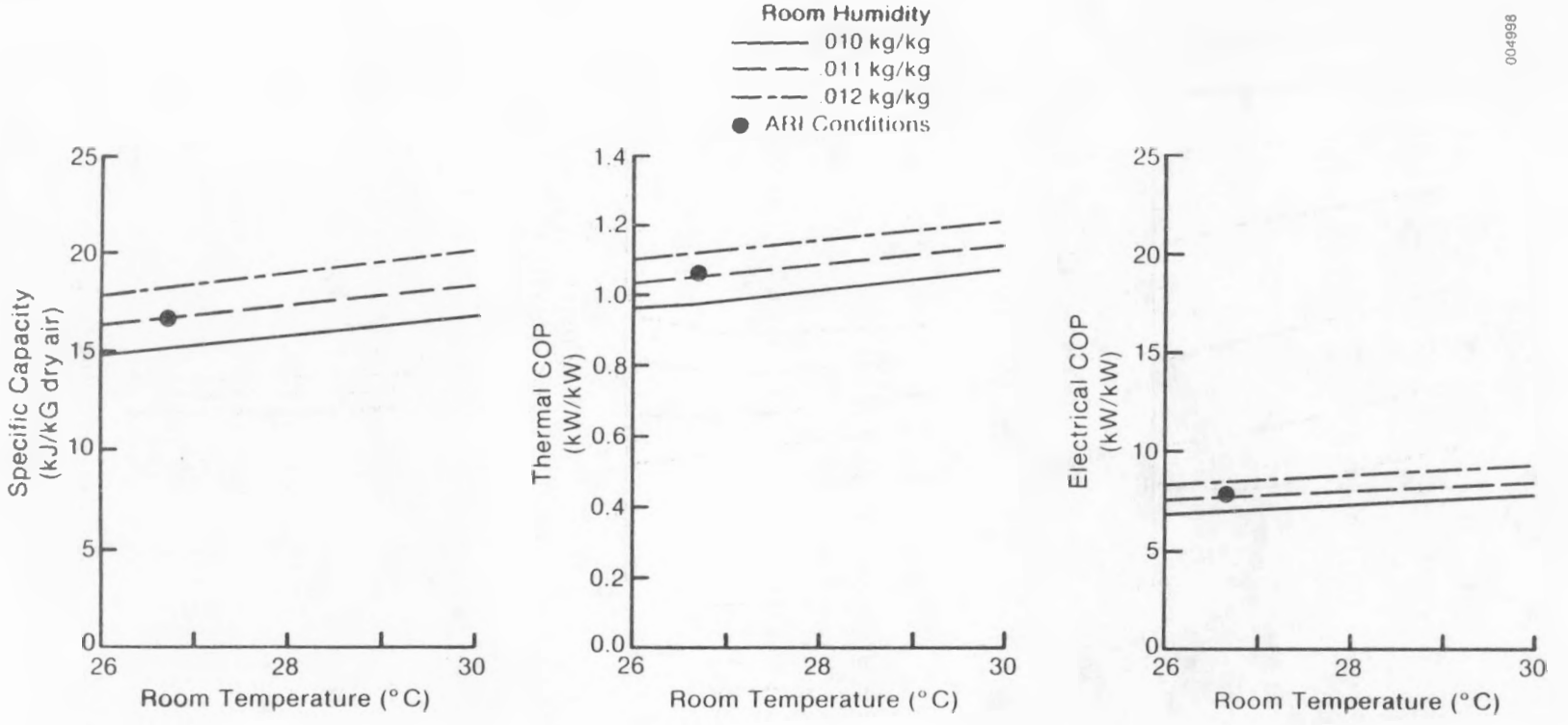

Figure 6-2. System Performance versus Room Conditions

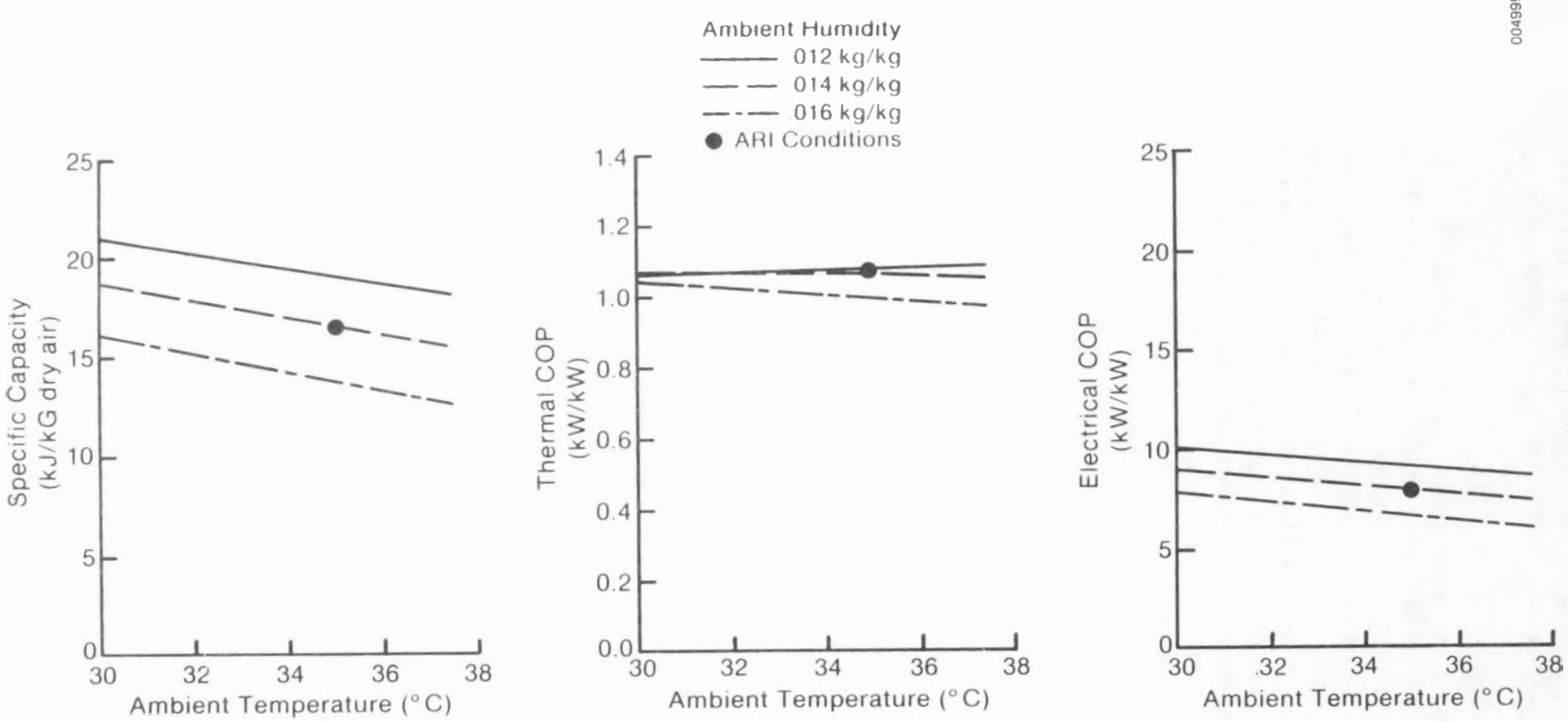

Figure 6-3. System Performance versus Ambient Conditions

design point by 15% does the effect appear. Ambient conditions have a linear effect on capacity (and hence electrical COP) because the fixed inventory of desiccant must deal with a proportionately higher moisture removal rate, a factor that could be mitigated by controlling the rotation speed of the wheel.

Regeneration temperature is one of the most important process variables of the desiccant cooling system. Figure 6-4 illustrates the effects of air supply temperature on system performance. Specific capacity is strongly affected because this temperature determines the degree of dryness to which the bed can be regenerated, and hence its capacity to remove moisture from the adsorption side at a given rotation speed. Therefore, higher regeneration temperature means a dryer bed and higher capacity. Thermal COP reaches a peak between 60°C and 80°C, because of a diminishing beneficial effect from the regeneration preheat supplied by the heat exchanger. An optimization of system design must trade off the capacity gains of higher regeneration temperature with the losses in thermal COP.

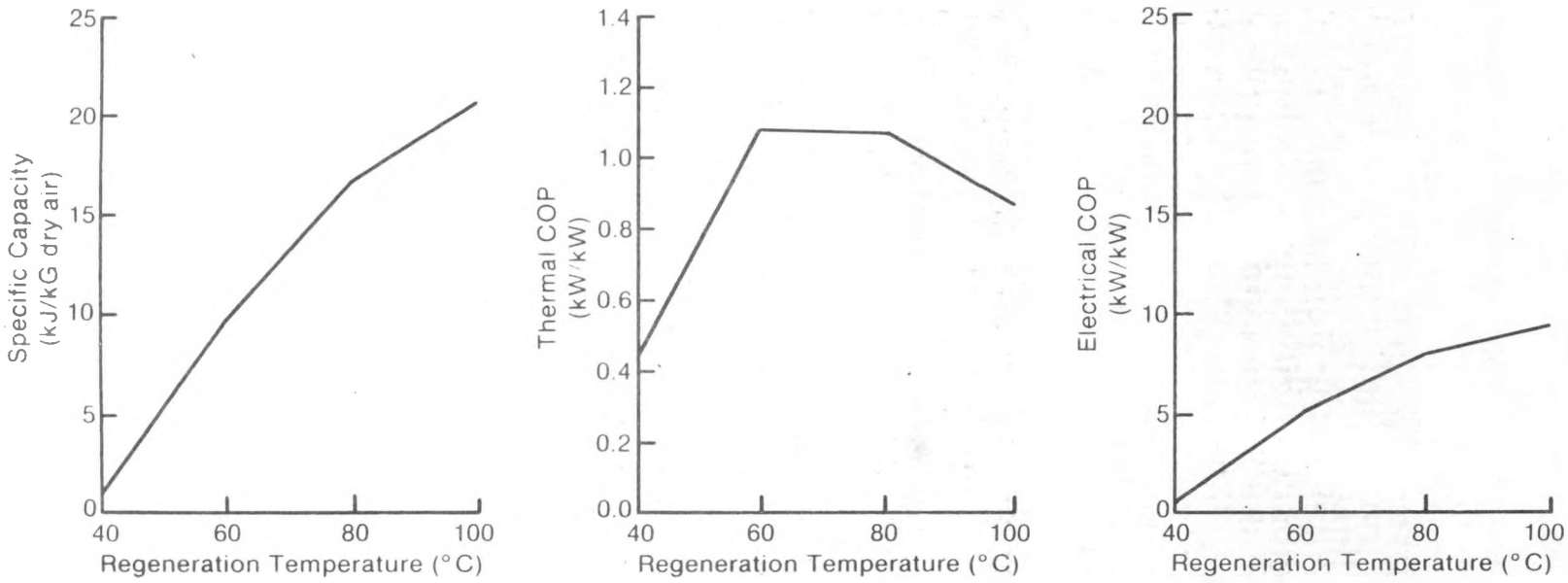

Figure 6-4. System Performance versus Regeneration Temperature

SECTION 7.0

CONCLUSIONS AND RECOMMENDATIONS

Research designed to identify a high-performance dehumidifier has produced a parallel-passage design that is simple to build and uses only commonly available materials of construction. The laboratory prototype performed well in adsorption and regeneration tests, with very low pressure drop at design flow rates. It was found that a narrow channel-flow geometry with very small silica gel desiccant particles is a near-optimum design. The DESSIM model, validated by the experimental data, predicts system performance of 1.07 thermal COP, 7.9 electrical COP (27 EER), and 16.7 kJ/kg dry air specific capacity, based on the dehumidifier design. Effects of room and ambient conditions as well as regeneration temperature have been quantified.

The next step in the development of the parallel-passage dehumidifier is verification of its performance in the cyclic operation typical of a solar desiccant cooling system. This experimental work should address several areas that will affect the performance of the dehumidifier in a system:

- Mechanical stability under thermal expansion and contraction stresses between adsorption and regeneration airstreams
- Effects of adsorption/desorption hysteresis on the dehumidifier's effectiveness
- Appropriate materials of construction
- Sealing between process airstreams.

Further evaluations should be made of system performance using the advanced dehumidifier design. Improvements in performance could be obtained by considering unbalanced flow rates in adsorption and regeneration airstreams, purge streams to cool the bed before entering the adsorption airstream, and changes in matrix design parameters, such as the heat capacity of the bed. Incorporating the parallel-passage dehumidifier into a hybrid system that combines desiccant cooling with vapor-compression chilling should be investigated to achieve performance improvements and savings in size and cost.

SECTION 8.0

REFERENCES

1. Rousseau, J., Development of a Solar Desiccant Dehumidifier-Final Summary Report, AiResearch Report 82-18944, Torrance, CA: Garrett AiResearch Manufacturing Company, November 1982.

2. Macriss, R. A., J. Wurm, T. Zawacki, and J. A. Keriast, Solar-MEC Development Program-Final Report, Chicago, IL: Institute of Gas Technology, July 1982.

3. Monnier, J.-B., W. M. Worek, and Z. Lavan, Testing of a Cross-Cooled Solar-Powered Desiccant Cooling System, DES-82-1, Chicago, IL: Illinois Institute of Technology, Mechanical Engineering Dept., January 1982.

4. Booz-Allen & Hamilton, Evaluation of Residential and Commercial Solar/Gas Heating and Cooling Technologies, GRI-79/0105, Chicago, IL: Gas Research Institute, 1981.

5. Barlow, R., Analysis of the Adsorption Process and of Desiccant Cooling Systems - A Pseudo-Steady-State Model for Coupled Heat and Mass Transfer, SERI/TR-631-1330, Golden, CO: Solar Energy Research Institute, December 1982.

6. Barlow, R., An Assessment of Dehumidifier Geometries for Desiccant Cooling Systems, SERI/TR-252-1529, Golden, CO: Solar Energy Research Institute, March 1982.

7. Kutscher, C. F., and R. S. Barlow, Dynamic Performance of Packed Bed Dehumidifiers: Experimental Results from the SERI Desiccant Test Laboratory, SERI/TR-252-1429, Golden, CO: Solar Energy Research Institute, March 1982.

8. Dunkle, R. V., et al., "Wound Parallel Plate Exchangers for Air-Conditioning Applications." Compact Heat Exchangers - History, Technological Advancement and Mechanical Design Problems, American Society of Mechanical Engineers HTD, Vol. 10, October 1980, pp. 65-71.

9. Kim, S., "Development of a Laminar Flow Desiccant Bed for Solar Air Conditioning Application," M.S. Thesis, Los Angeles, CA: University of California at Los Angeles, 1981.

10. Biswas, P., "An Experimental Study of the Performance of a Laminar Flow Silica Gel Desiccant Packing Suitable for Solar Air Conditioning Application." M.S. Thesis, Los Angeles, CA: University of California at Los Angeles, 1981.

11. Jurinak, J., "Open-Cycle Solid Desiccant Cooling - Component Models and System Simulations," Ph.D. Thesis, Madison, WI: University of Wisconsin, 1982.

12. Barlow, R., and K. Collier, "Optimizing the Performance of Deisccant Beds for Solar Regenerated Cooling," Proceedings of the AS/ISES Annual Conference, SERI/TP-631-1157, May 1981.

13. Roja, F. "Pure Vapor Adsorption of Water on Silica Gels of Different Porosity," M.S. Thesis 2342, Golden, CO: Colorado School of Mines, 1980.

14. Davison Silica Gels, Baltimore, MD: W. R. Grance & Co.

15. Holman, J. P., Heat Transfer, New York, NY: McGraw-Hill Book Company, 1972.

16. Kays, W. M., and A. L. London, Compact Heat Exchangers, New York, NY: McGraw Hill Book Company, 1964.

APPENDIX

EXPERIMENTAL RESULTS

Experimental data and results predicted by the DESSIM performance model are presented for each run. Experimental data of inlet/outlet temperature and humidity, represented by point data, were plotted during the actual run. The predicted temperature and humidity, represented by solid and dashed lines, respectively, are superimposed on the experimental data for comparison.

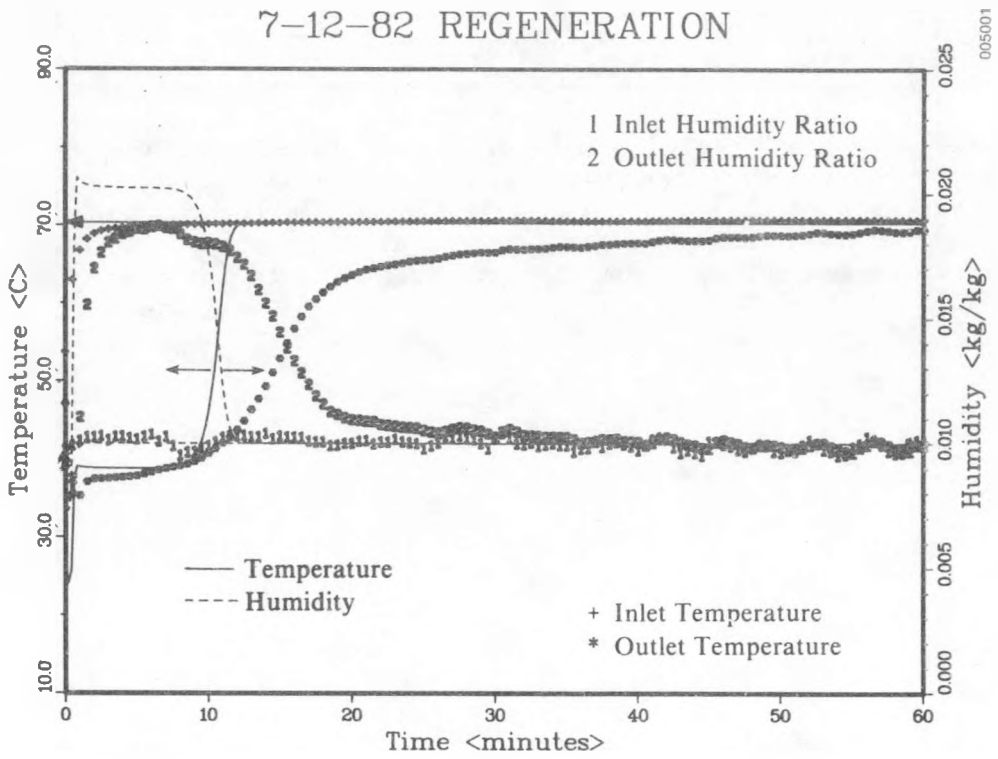
7-12-82 REGENERATION
005001
1 Inlet Humidity Ratio
2 Outlet Humidity Ratio
Temperature
Humidity
+ Inlet Temperature
* Outlet Temperature
Temperature <C>
Humidity <kg/kg>
Time <minutes>
90.0
70.0
50.0
30.0
10.0
0.025
0.020
0.015
0.010
0.005
0.000
0
10
20
30
40
50
60

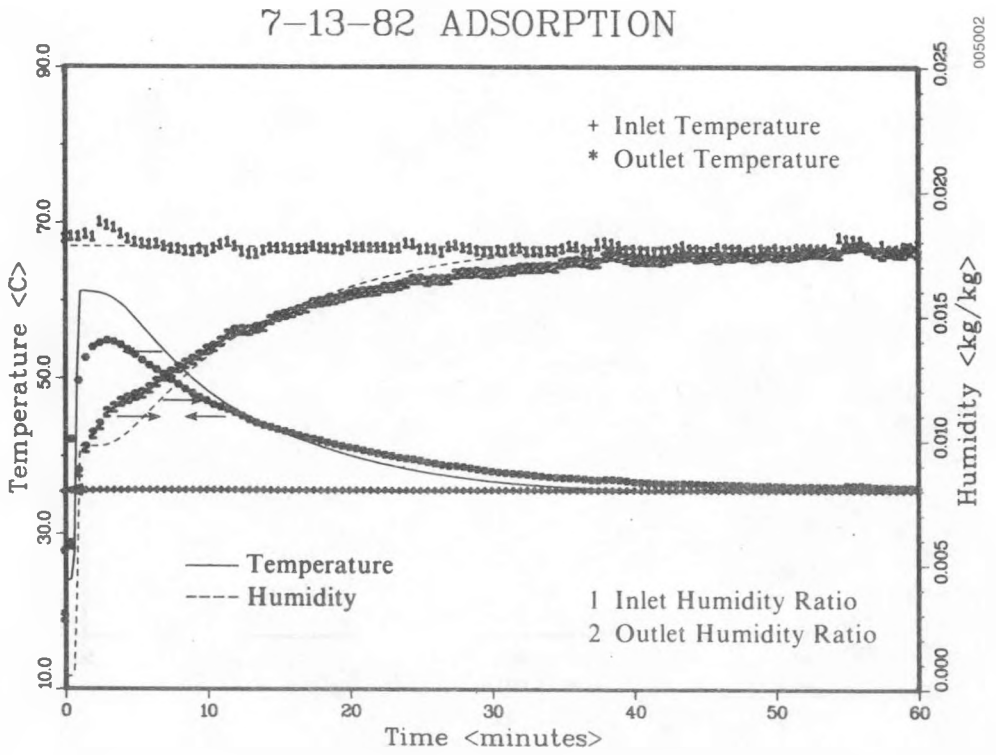
7-13-82 ADSORPTION
005002
+ Inlet Temperature
* Outlet Temperature
Temperature
Humidity
1 Inlet Humidity Ratio
2 Outlet Humidity Ratio
Temperature <C>
Humidity <kg/kg>
Time <minutes>
90.0
70.0
50.0
30.0
10.0
0.025
0.020
0.015
0.010
0.005
0.000
0
10
20
30
40
50
60

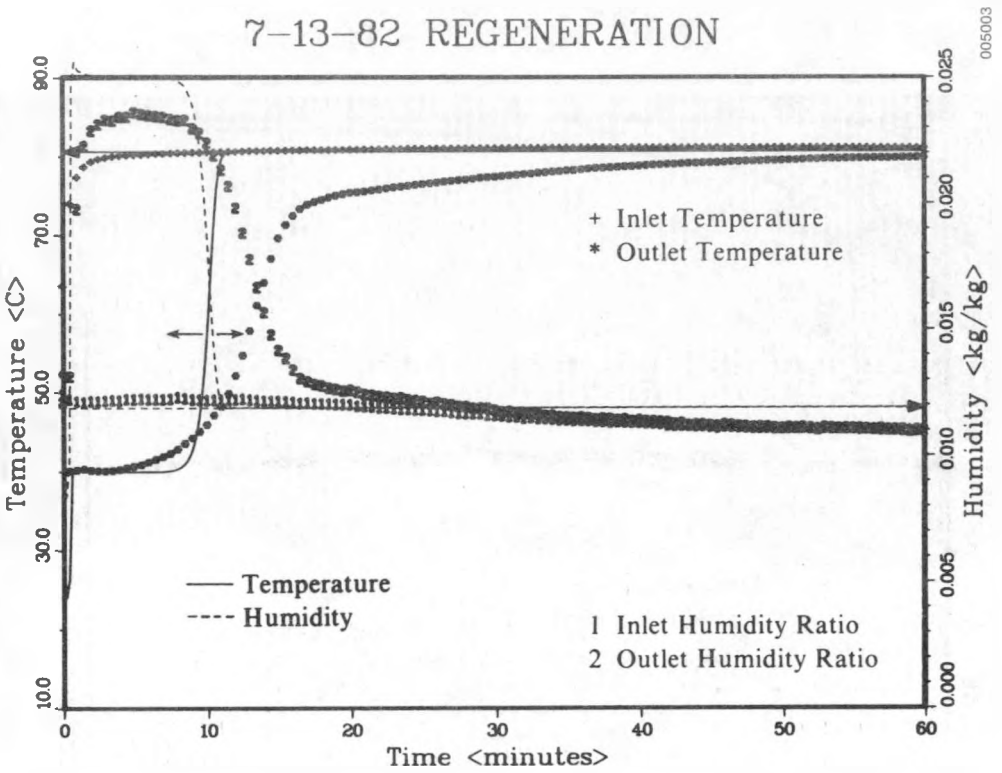
7-13-82 REGENERATION
005003
Temperature <C>
Humidity <kg/kg>
Time <minutes>
+ Inlet Temperature
* Outlet Temperature
Temperature
Humidity
1 Inlet Humidity Ratio
2 Outlet Humidity Ratio

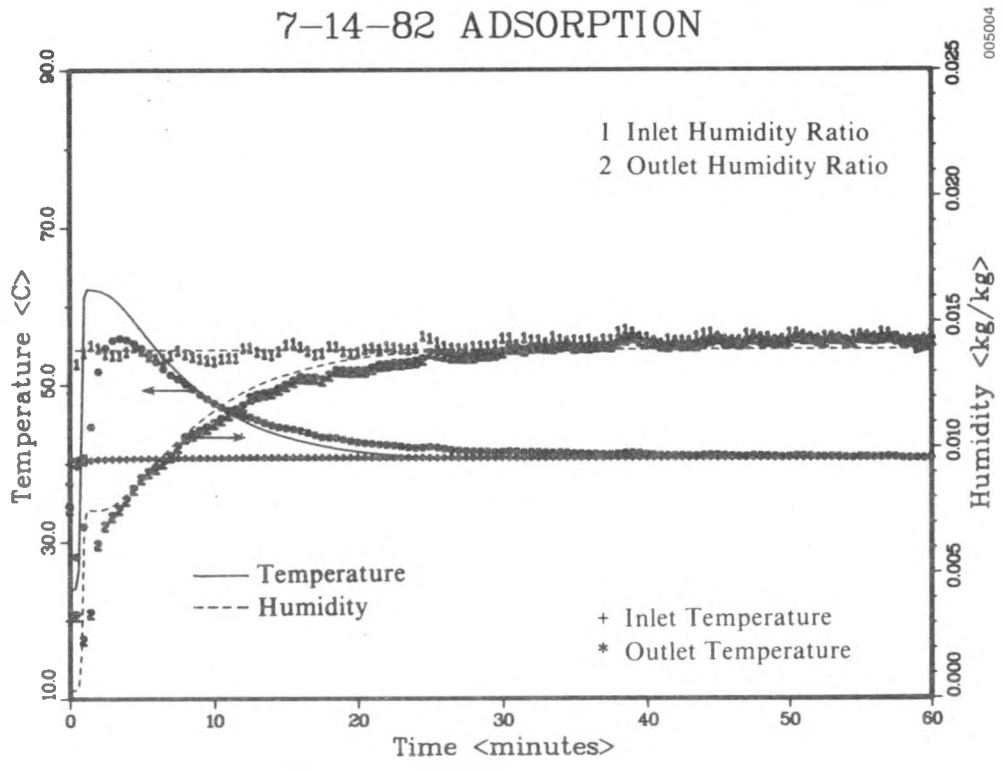
7-14-82 ADSORPTION
005004
Temperature <C>
Humidity <kg/kg>
Time <minutes>
1 Inlet Humidity Ratio
2 Outlet Humidity Ratio
Temperature
Humidity
+ Inlet Temperature
* Outlet Temperature

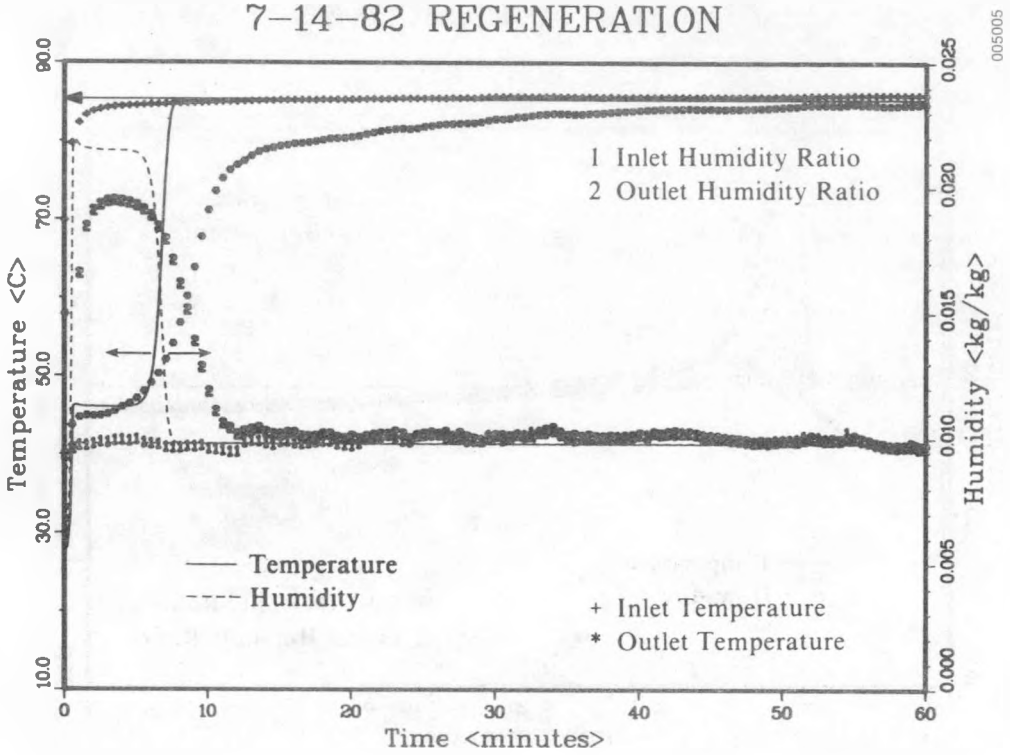
7-14-82 REGENERATION
005005
1 Inlet Humidity Ratio
2 Outlet Humidity Ratio
Temperature
Humidity
+ Inlet Temperature
* Outlet Temperature
Temperature <C>
Humidity <kg/kg>
Time <minutes>
90.0
70.0
50.0
30.0
10.0
0.025
0.020
0.015
0.010
0.005
0.000
0
10
20
30
40
50
60

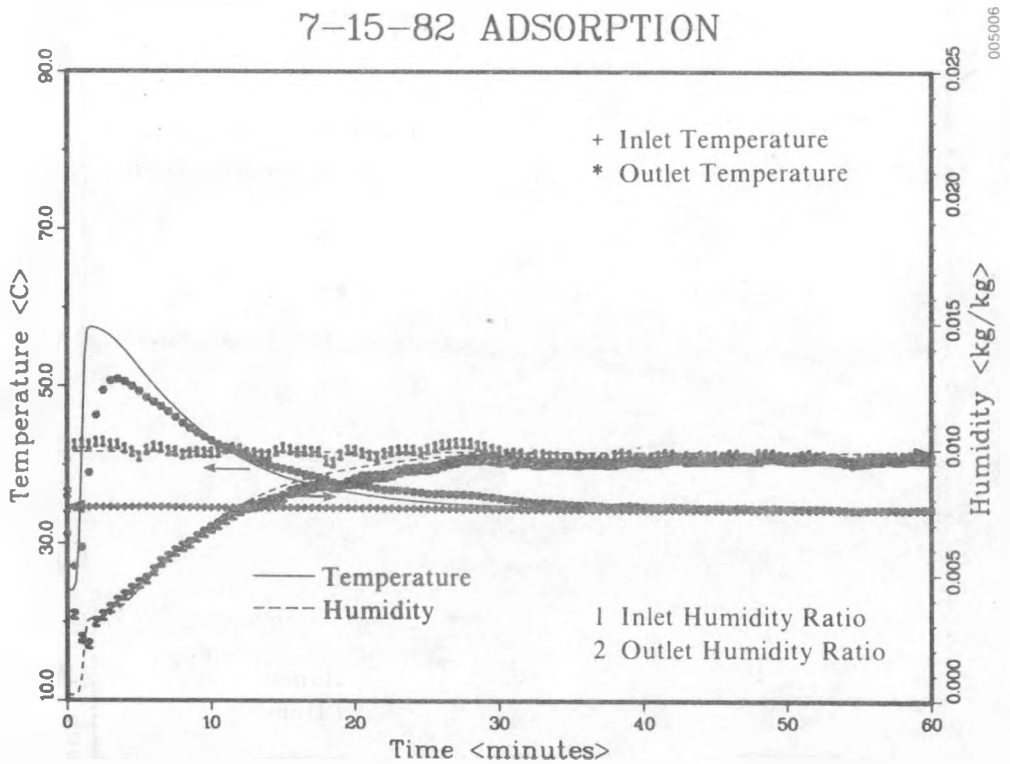
7-15-82 ADSORPTION
005006
+ Inlet Temperature
* Outlet Temperature
Temperature
Humidity
1 Inlet Humidity Ratio
2 Outlet Humidity Ratio
Temperature <C>
Humidity <kg/kg>
Time <minutes>
90.0
70.0
50.0
30.0
10.0
0.025
0.020
0.015
0.010
0.005
0.000
0
10
20
30
40
50
60

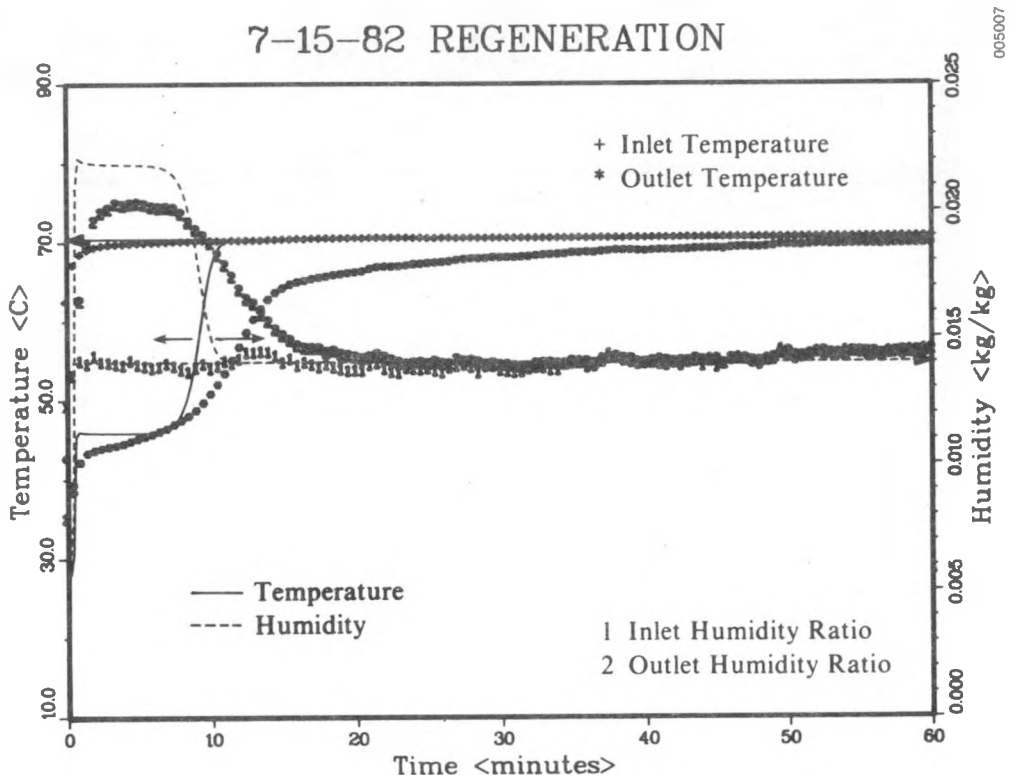
7-15-82 REGENERATION
005007
+ Inlet Temperature
* Outlet Temperature
Temperature
Humidity
1 Inlet Humidity Ratio
2 Outlet Humidity Ratio
Temperature <C>
Humidity <kg/kg>
Time <minutes>
90.0
70.0
50.0
30.0
10.0
0.025
0.020
0.015
0.010
0.005
0.000
0
10
20
30
40
50
60

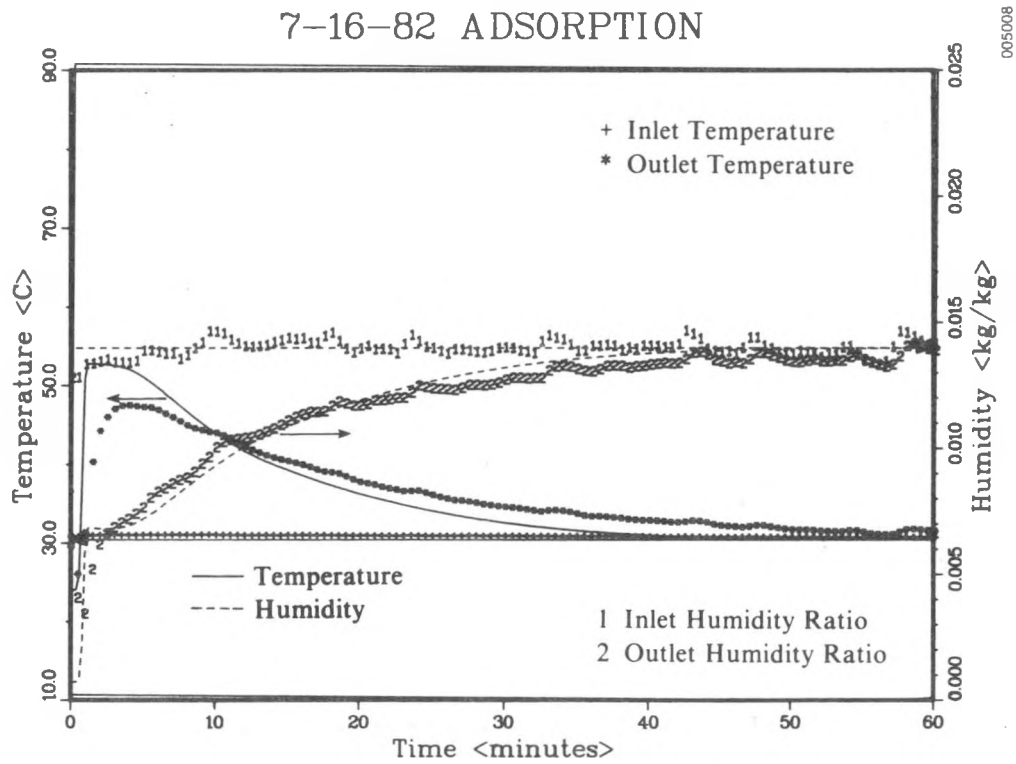
7-16-82 ADSORPTION
005008
+ Inlet Temperature
* Outlet Temperature
Temperature
Humidity
1 Inlet Humidity Ratio
2 Outlet Humidity Ratio
Temperature <C>
Humidity <kg/kg>
Time <minutes>
90.0
70.0
50.0
30.0
10.0
0.025
0.020
0.015
0.010
0.005
0.000
0
10
20
30
40
50
60

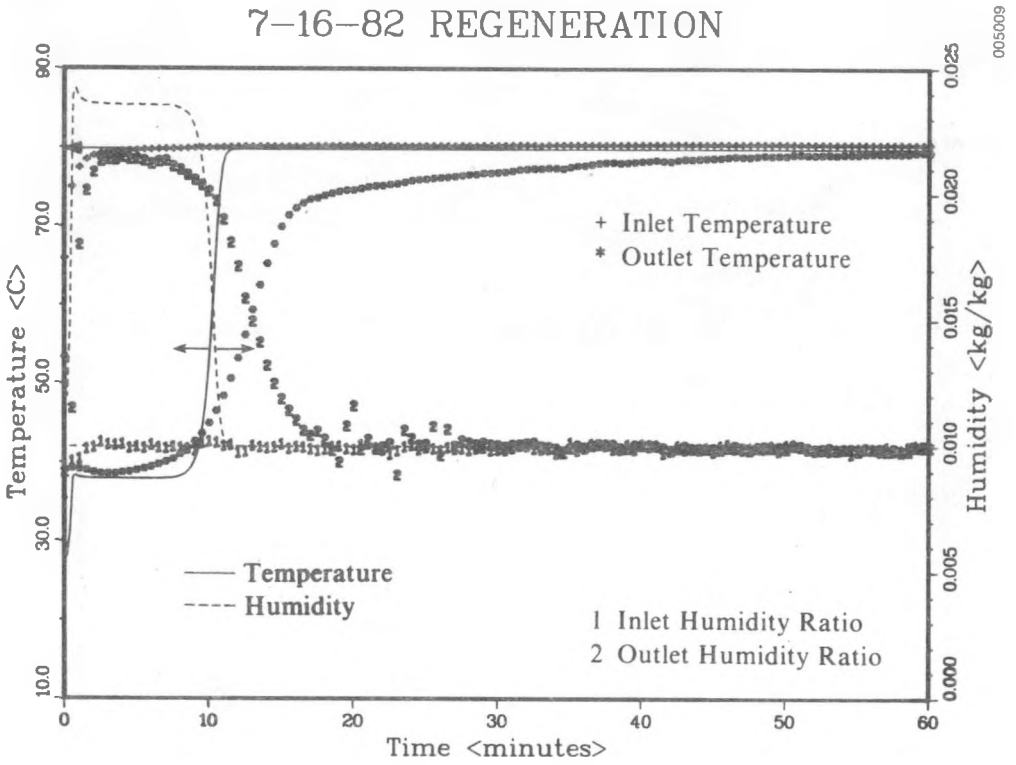
7-16-82 REGENERATION
005009
Temperature <C>
Humidity <kg/kg>
Time <minutes>
+ Inlet Temperature
* Outlet Temperature
Temperature
Humidity
1 Inlet Humidity Ratio
2 Outlet Humidity Ratio

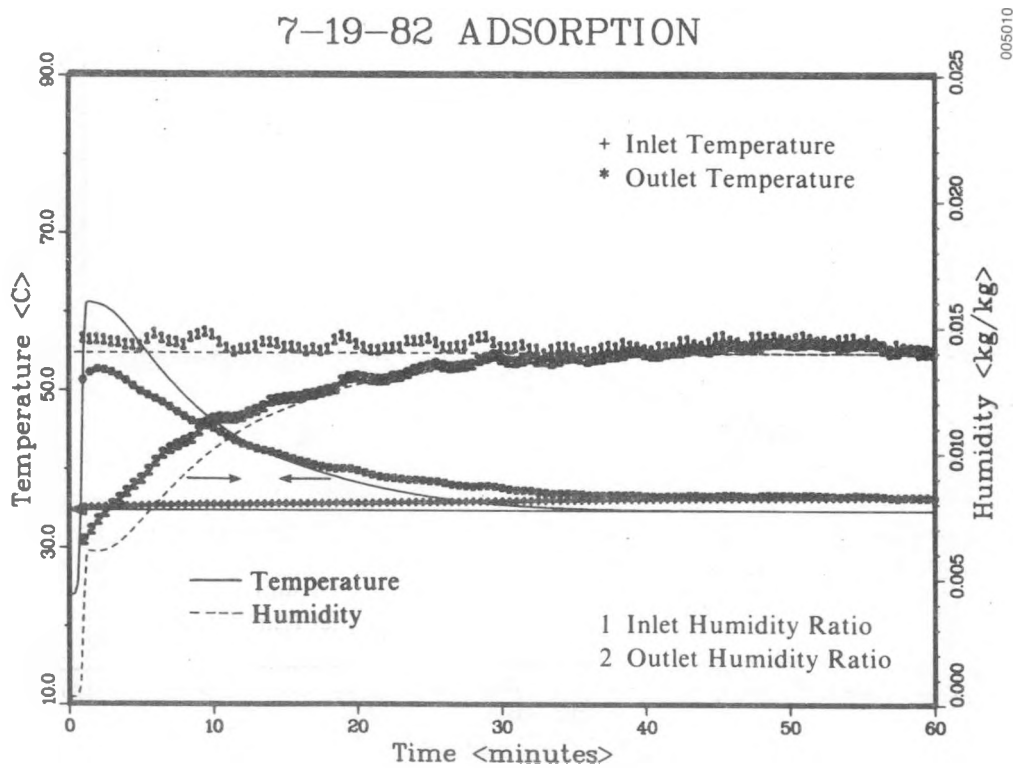
7-19-82 ADSORPTION
005010
Temperature <C>
Humidity <kg/kg>
Time <minutes>
+ Inlet Temperature
* Outlet Temperature
Temperature
Humidity
1 Inlet Humidity Ratio
2 Outlet Humidity Ratio

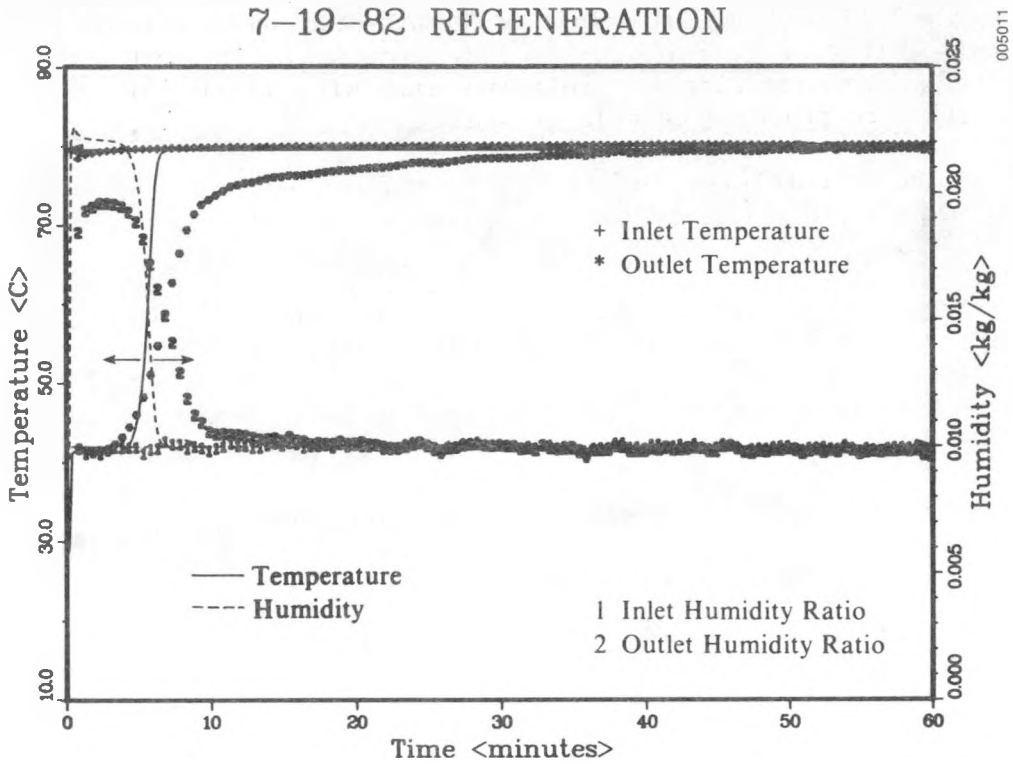
7-19-82 REGENERATION
005011
+ Inlet Temperature
* Outlet Temperature
Temperature
Humidity
1 Inlet Humidity Ratio
2 Outlet Humidity Ratio
Temperature <C>
Humidity <kg/kg>
Time <minutes>
90.0
70.0
50.0
30.0
10.0
0.025
0.020
0.015
0.010
0.005
0.000
0
10
20
30
40
50
60

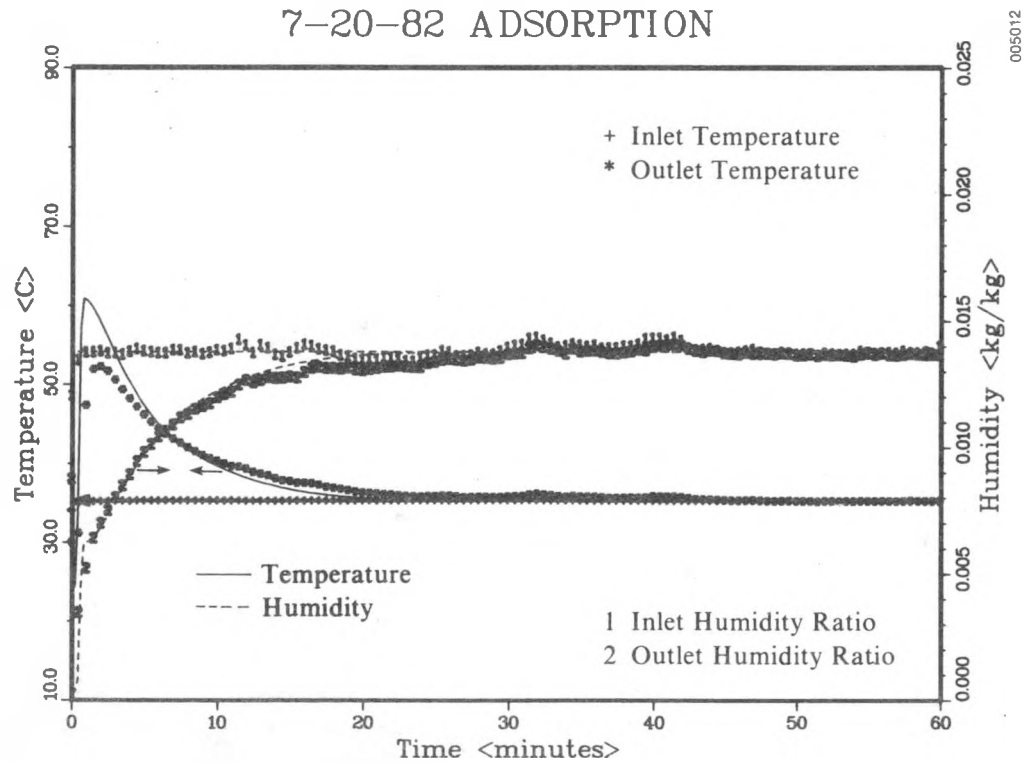
7-20-82 ADSORPTION
005012
+ Inlet Temperature
* Outlet Temperature
Temperature
Humidity
1 Inlet Humidity Ratio
2 Outlet Humidity Ratio
Temperature <C>
Humidity <kg/kg>
Time <minutes>
90.0
70.0
50.0
30.0
10.0
0.025
0.020
0.015
0.010
0.005
0.000
0
10
20
30
40
50
60

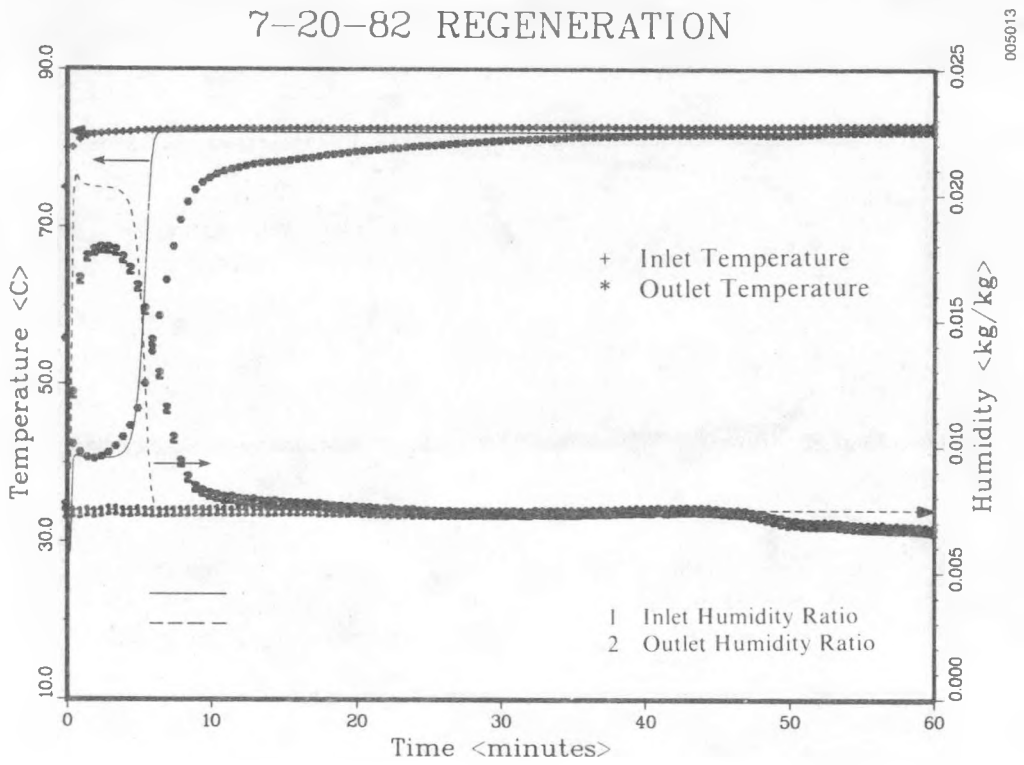
7-20-82 REGENERATION
005013
Temperature <C>
Humidity <kg/kg>
Time <minutes>
+ Inlet Temperature
* Outlet Temperature
1 Inlet Humidity Ratio
2 Outlet Humidity Ratio
90.0
70.0
50.0
30.0
10.0
0.025
0.020
0.015
0.010
0.005
0.000
0
10
20
30
40
50
60

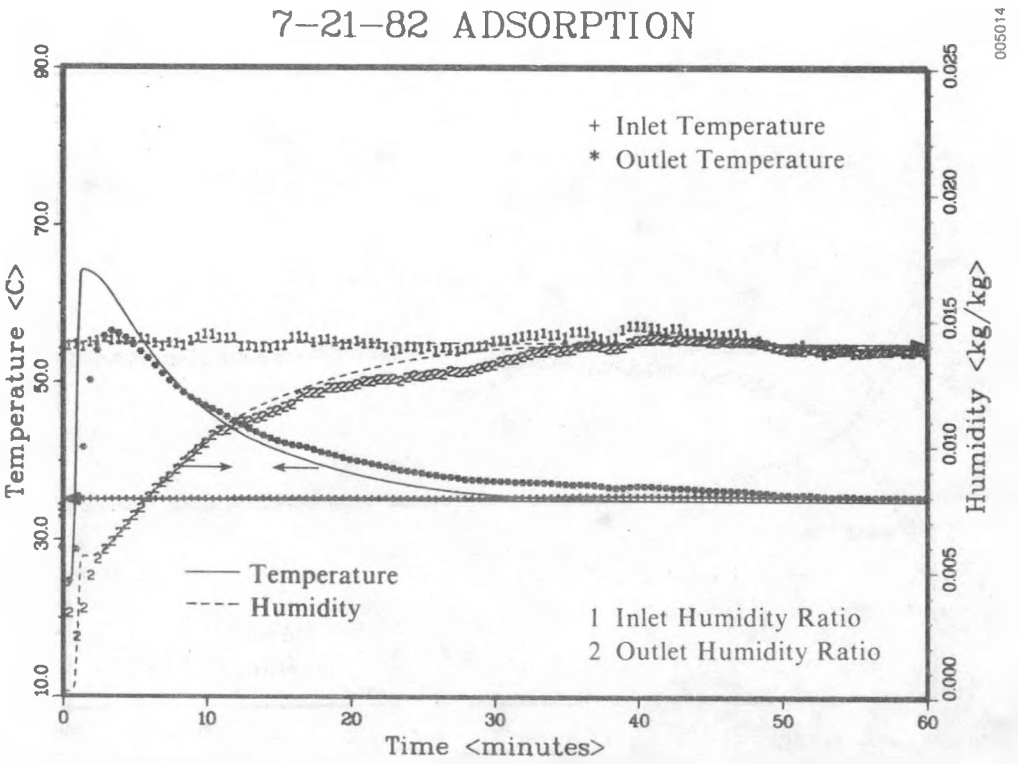
7-21-82 ADSORPTION
005014
Temperature <C>
Humidity <kg/kg>
Time <minutes>
+ Inlet Temperature
* Outlet Temperature
Temperature
Humidity
1 Inlet Humidity Ratio
2 Outlet Humidity Ratio
90.0
70.0
50.0
30.0
10.0
0.025
0.020
0.015
0.010
0.005
0.000
0
10
20
30
40
50
60

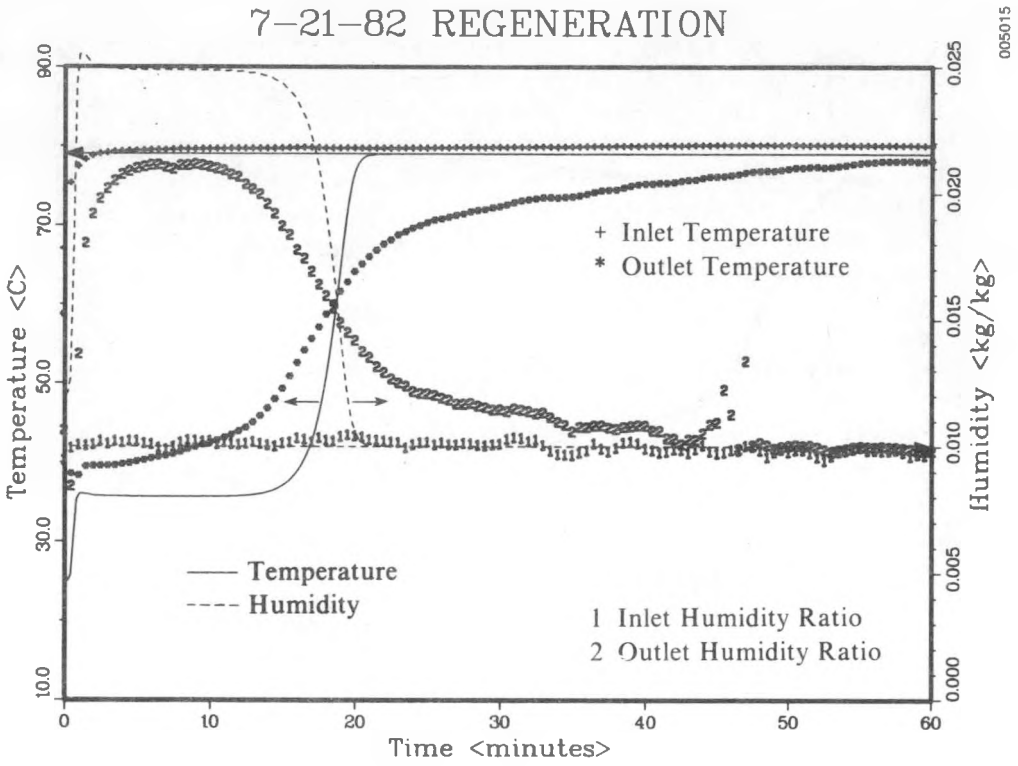
7-21-82 REGENERATION
005015
Temperature <C>
Humidity <kg/kg>
Time <minutes>
+ Inlet Temperature
* Outlet Temperature
Temperature
Humidity
1 Inlet Humidity Ratio
2 Outlet Humidity Ratio

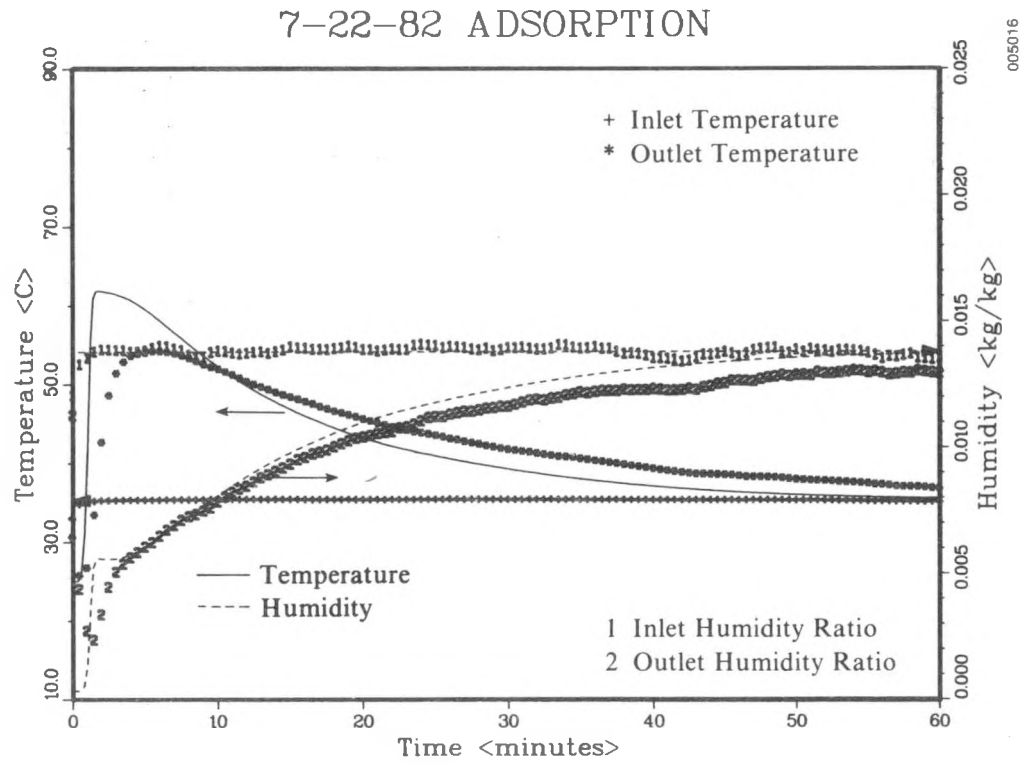
7-22-82 ADSORPTION
005016
Temperature <C>
Humidity <kg/kg>
Time <minutes>
+ Inlet Temperature
* Outlet Temperature
Temperature
Humidity
1 Inlet Humidity Ratio
2 Outlet Humidity Ratio

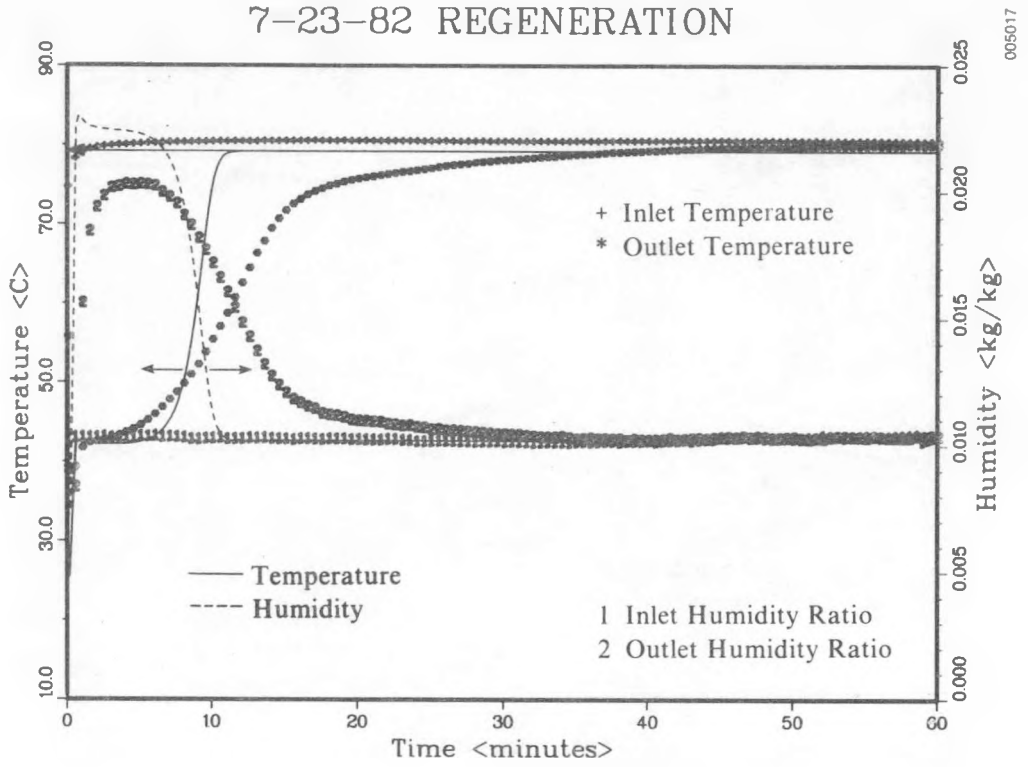
7-23-82 REGENERATION
005017
Temperature <C>
Humidity <kg/kg>
Time <minutes>
+ Inlet Temperature
* Outlet Temperature
Temperature
Humidity
1 Inlet Humidity Ratio
2 Outlet Humidity Ratio

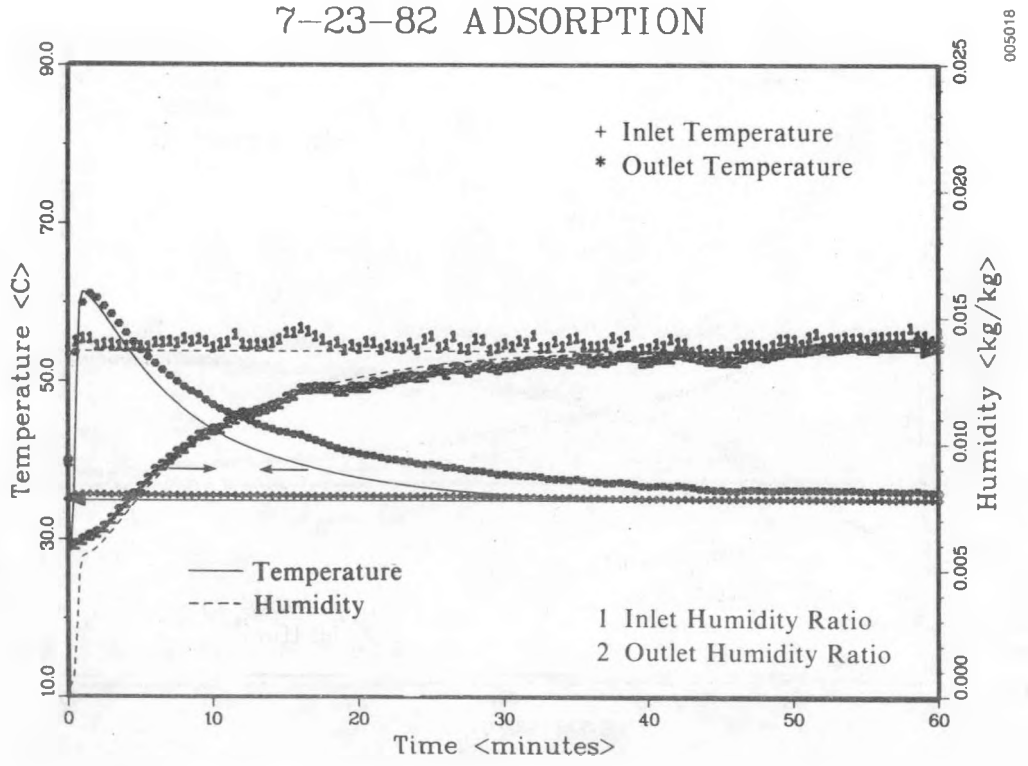
7-23-82 ADSORPTION
005018
Temperature <C>
Humidity <kg/kg>
Time <minutes>
+ Inlet Temperature
* Outlet Temperature
Temperature
Humidity
1 Inlet Humidity Ratio
2 Outlet Humidity Ratio

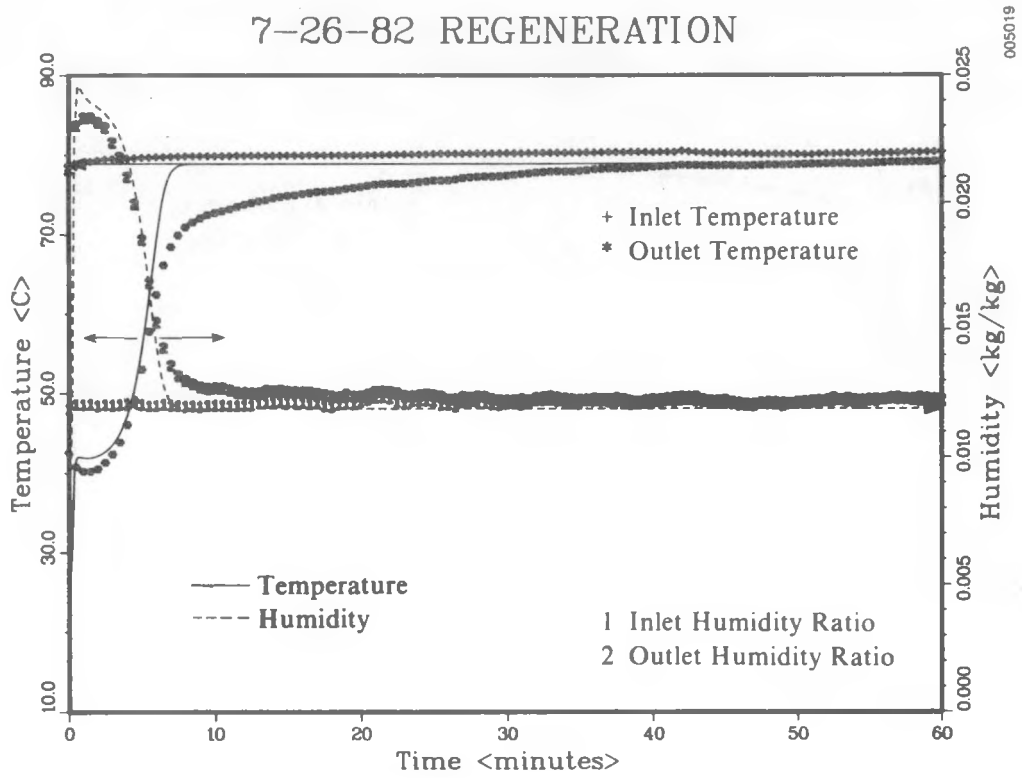
7-26-82 REGENERATION
005019
Temperature <C>
Humidity <kg/kg>
Time <minutes>
+ Inlet Temperature
* Outlet Temperature
Temperature
Humidity
1 Inlet Humidity Ratio
2 Outlet Humidity Ratio

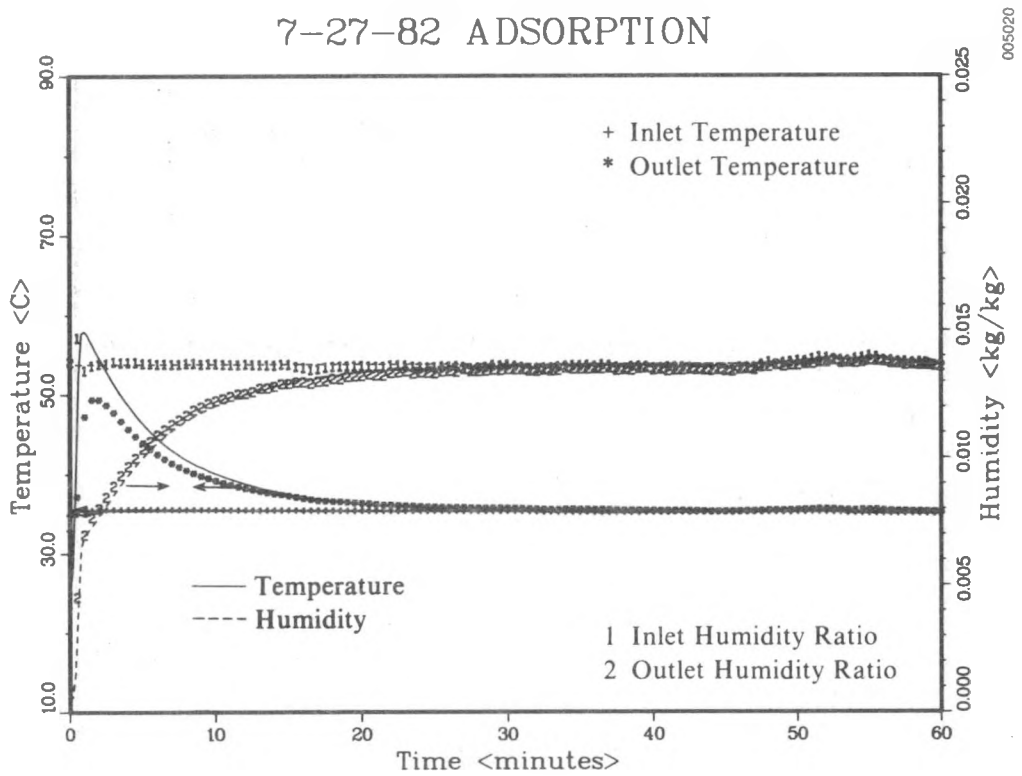
7-27-82 ADSORPTION
005020
Temperature <C>
Humidity <kg/kg>
Time <minutes>
+ Inlet Temperature
* Outlet Temperature
Temperature
Humidity
1 Inlet Humidity Ratio
2 Outlet Humidity Ratio

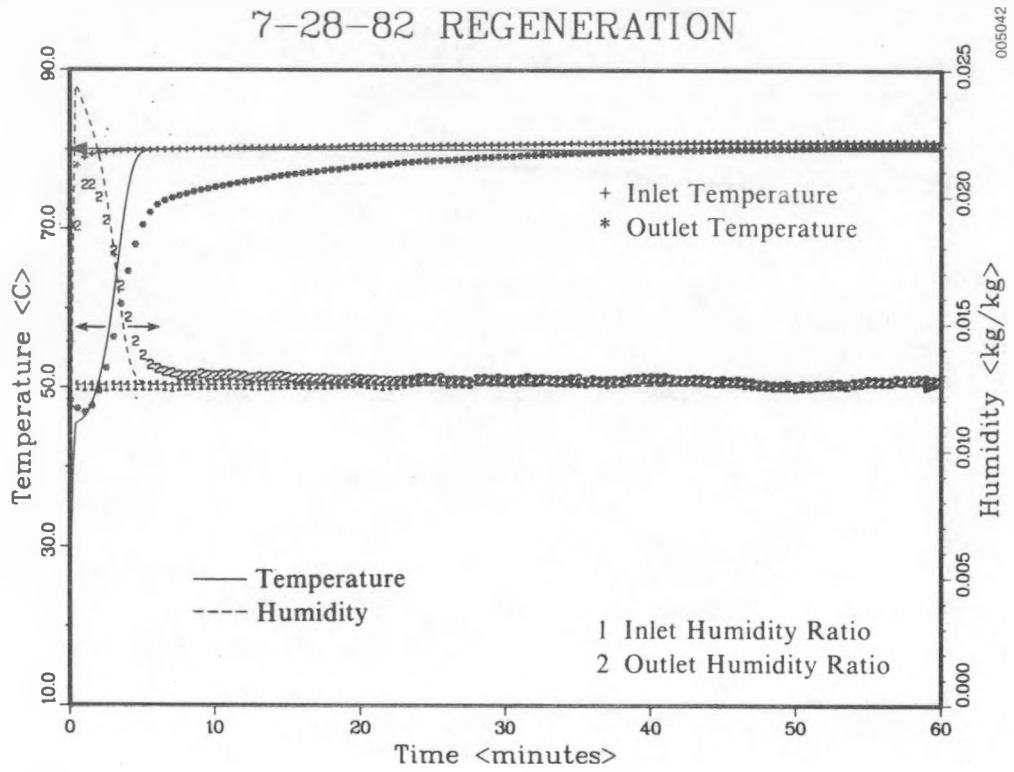
7-28-82 REGENERATION
005042
+ Inlet Temperature
* Outlet Temperature
Temperature
Humidity
1 Inlet Humidity Ratio
2 Outlet Humidity Ratio
Temperature <C>
Humidity <kg/kg>
Time <minutes>
90.0
70.0
50.0
30.0
10.0
0.025
0.020
0.015
0.010
0.005
0.000
0
10
20
30
40
50
60

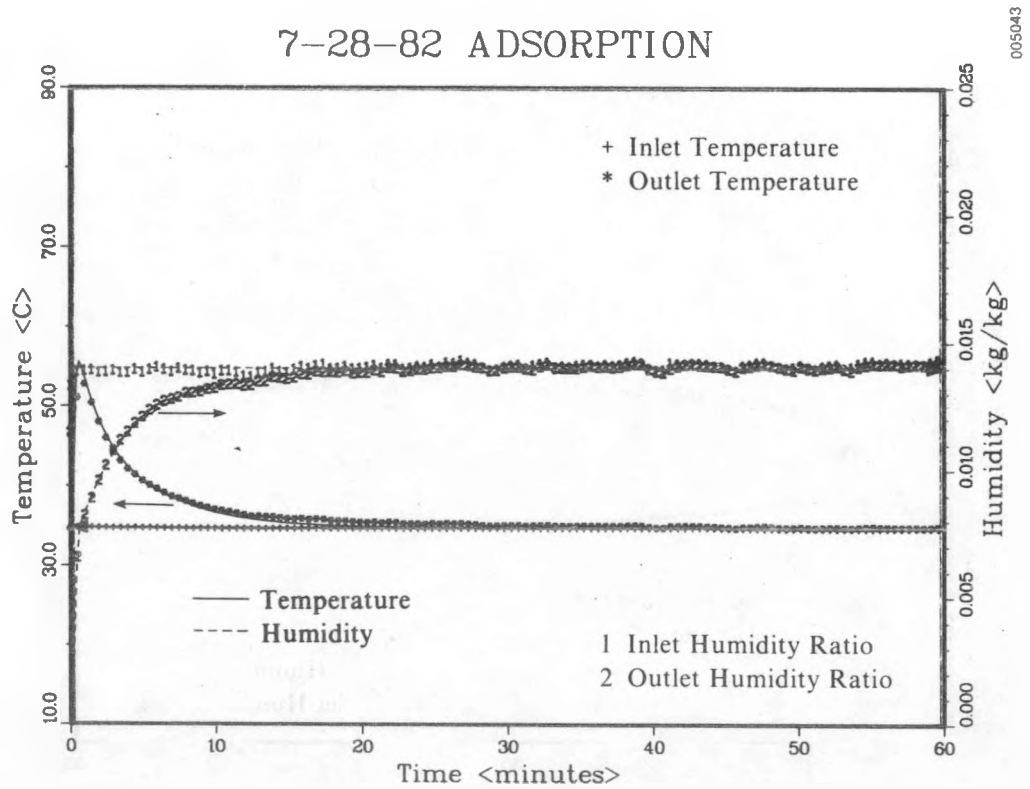
7-28-82 ADSORPTION
005043
+ Inlet Temperature
* Outlet Temperature
Temperature
Humidity
1 Inlet Humidity Ratio
2 Outlet Humidity Ratio
Temperature <C>
Humidity <kg/kg>
Time <minutes>
90.0
70.0
50.0
30.0
10.0
0.025
0.020
0.015
0.010
0.005
0.000
0
10
20
30
40
50
60

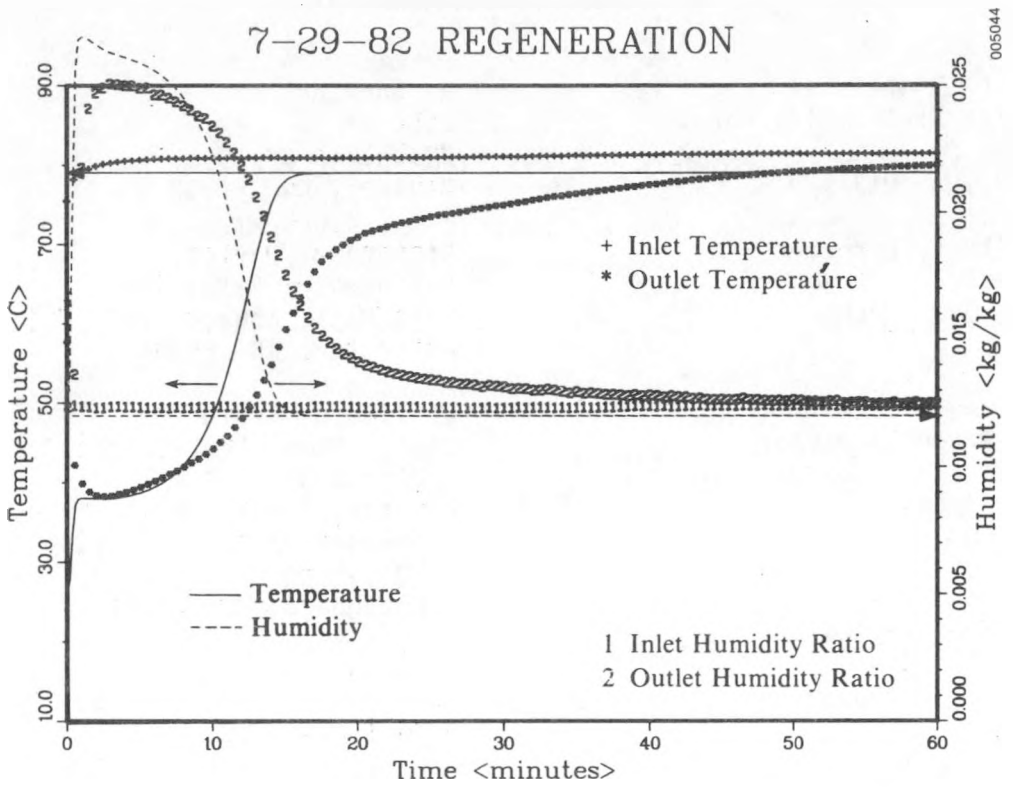
7-29-82 REGENERATION
005044
Temperature <C>
Humidity <kg/kg>
Time <minutes>
+ Inlet Temperature
* Outlet Temperature
Temperature
Humidity
1 Inlet Humidity Ratio
2 Outlet Humidity Ratio

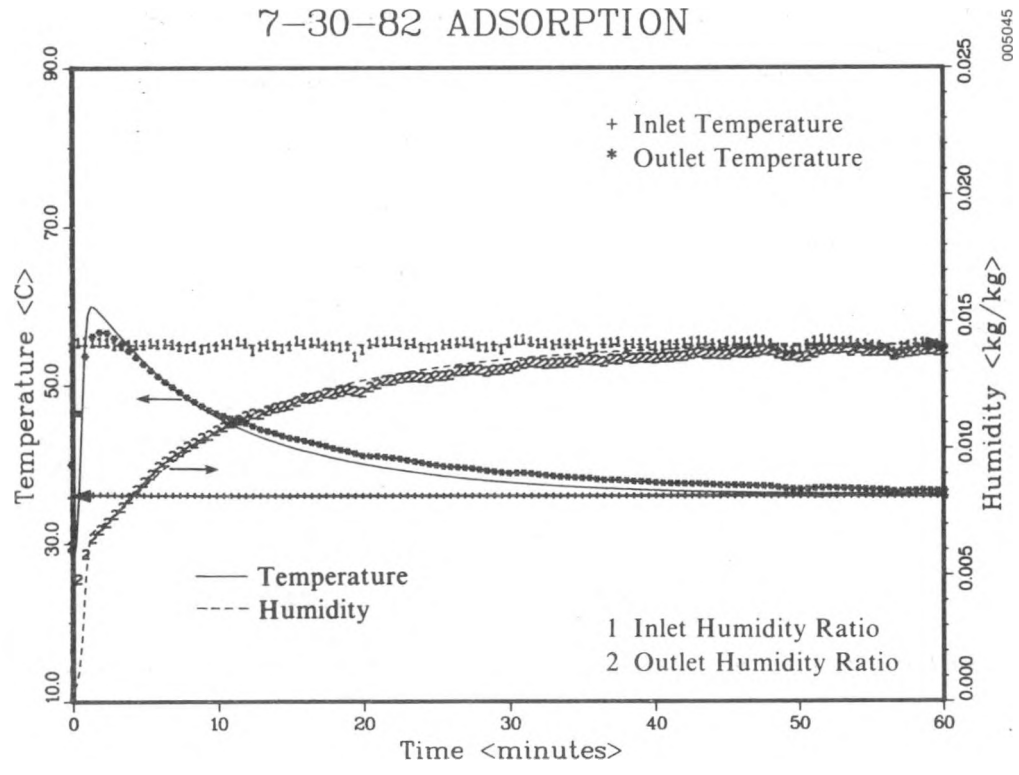
7-30-82 ADSORPTION
005045
Temperature <C>
Humidity <kg/kg>
Time <minutes>
+ Inlet Temperature
* Outlet Temperature
Temperature
Humidity
1 Inlet Humidity Ratio
2 Outlet Humidity Ratio